Quaternary Science Reviews 130 (2015) 89–108

Contents lists available at ScienceDirect

Quaternary Science Reviews

journal homepage: www.elsevier.com/locate/quascirev

Causal links between Nile floods and eastern Mediterranean sapropel formation during the past 125 kyr confirmed by OSL and radiocarbon dating of Blue and White Nile sediments

M.A.J. Williams [a, *], G.A.T. Duller [b], F.M. Williams [c], J.C. Woodward [d], M.G. Macklin [b], O.A.M. El Tom [e], R.N. Munro [f], Y. El Hajaz [g], T.T. Barrows [h]

[a] Earth Sciences, University of Adelaide, Adelaide, SA 5005, Australia
[b] Institute of Geography and Earth Sciences, Aberystwyth University, Aberystwyth, Ceredigion SY23 3DB, UK
[c] Environmental Luminescence, School of Chemistry and Physics, University of Adelaide, Adelaide 5005, Australia
[d] The University of Manchester, Geography, School of Environment & Development, Manchester M13 9PL, UK
[e] Land & Water Research Centre, Agricultural Research & Technology Corporation, PO Box 216, Wad Medani, Sudan
[f] Department of Earth & Environmental Sciences, K.U. Leuven, Celestijnenlaan 200E-box 2411, 3001 Heverlee, Belgium
[g] Geology Department, International University of Africa, Khartoum, Sudan
[h] Geography Department, College of Life and Environmental Science, University of Exeter, Exeter, Devon EX4 4RJ, UK

ARTICLE INFO

Article history:
Received 31 December 2014
Received in revised form
18 May 2015
Accepted 27 May 2015
Available online 6 June 2015

Keywords:
Nile
Blue Nile
White Nile
Quaternary
Palaeochannels
Floods
Sapropels
Source-bordering dunes

ABSTRACT

It has long been hypothesised that beds of highly organic mud or sapropels seen in marine sediment cores retrieved from the floor of the eastern Mediterranean accumulated during times of high Nile fluvial discharge. Our recent fieldwork in the valleys of the Blue Nile, the White Nile and the main Nile has for the first time revealed a sequence of extreme flood episodes synchronous with sapropel units S5 (124 kyr), S4 (102 kyr), S3 (81 kyr), S2 (55 kyr) and S1 (13.5–6.5 kyr). There are more weakly defined links with Nile floods and sapropel units S9 (240 kyr), S8 (217 kyr), S7 (195 kyr), S6 (172 kyr), but the dating error terms are too large to allow us to be too definite. During times of extreme floods over the past 125 kyr, wide distributary channels of the Blue Nile flowed across the Gezira alluvial fan in central Sudan and transported a bed load of sand and gravel into the lower White Nile valley. The sands were reworked by wind to form source-bordering dunes, all of which contain heavy minerals of Ethiopian provenance. These source-bordering dunes were active at 115–105 kyr, 60 kyr and 12–7 kyr, all times of extreme Blue Nile floods. The flood and dune sediments were dated using a combination of optically stimulated luminescence (OSL) and radiocarbon analyses. The Quaternary record of Nile floods discussed here shows a precessional signal and reflects episodes of stronger summer monsoon and more northerly seasonal movement of the ITCZ, linked to times of higher insolation in northern tropical latitudes. Progressive aggradation of Holocene Nile channels in northern Sudan has had a profound influence upon human settlement in the last 8 kyr.

1. Introduction

The Nile is one of the world's great rivers (Fig. 1a). It is the longest river in the world (6690 km) and has the world's fourth largest catchment (2.8 million km^2). However, its annual flow (88,500 GL) is two orders of magnitude less than that of the Amazon (6,150,000 GL) and its annual yield (0.32 ML/ha) is only slightly more than that of the Murray-Darling (0.14 ML/ha), a river system similar to the Nile in also having a large and mostly arid to semi-arid catchment.

Garzanti et al. (2006) used the petrology of Nile sands in Sudan and Ethiopia to determine sediment budgets and erosion patterns in the three main tributaries of the Nile (White Nile, Blue Nile, Atbara). Padoan et al. (2011) extended this work, using the Sr and Nd isotopic composition together with heavy minerals and bulk petrography of Nile sediments (sands and muds) to identify the major sources of sediment throughout the Nile basin. They found that the Main Nile had an annual sediment yield of 77 ± 7 km^3, with

* Corresponding author.
E-mail address: martin.williams@adelaide.edu.au (M.A.J. Williams).

http://dx.doi.org/10.1016/j.quascirev.2015.05.024
0277-3791/

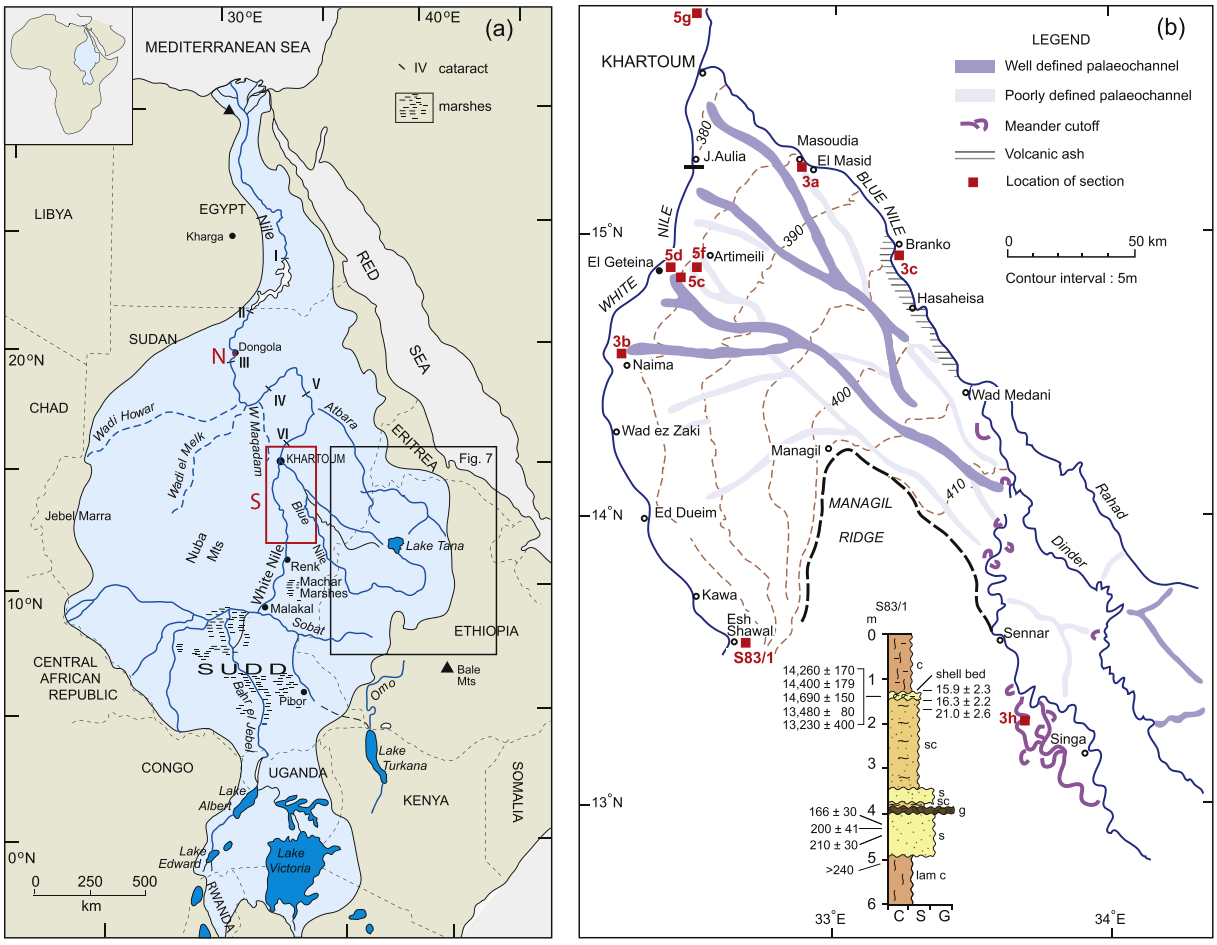

Fig. 1. a. Nile basin. S is the southern study area, shown in detail in Fig. 1b. N is the northern study area, shown in detail on Fig. 6. Inset square on right is Blue Nile and Atbara headwaters, shown in detail on Fig. 7. b. Southern study area showing Blue Nile Quaternary palaeochannels and location of certain dated stratigraphic sections.

roughly 70% of the suspended load derived from a volcanic source: the Ethiopian headwaters of the Atbara and Blue Nile (Figs. 1a and 7) but only about 39% of the bed load derived from volcanic rocks, in contrast to ~56% from metamorphic and ~5% from sedimentary sources. Although the catchment area of the White Nile is half that of the entire Nile basin and contributes a third of the total water discharge, its annual sediment contribution to the Main Nile (7×10^6 t) is trivial. This is because most of the present-day sediment is trapped in the lakes of Uganda, in the vast swamps of the Sudd and in the Machar marshes (Fig. 1a).

Three decades ago Rossignol-Strick and her colleagues proposed that the youngest *sapropel* unit in the eastern Mediterranean coincided with a time of very high early Holocene discharge from the Nile (Rossignol-Strick et al., 1982; Rossignol-Strick, 1985, 1999). (A *sapropel* is a layer of dark organic mud that formed under anoxic conditions on the floor of a lake or sea, in this case the Mediterranean). Since then a number of other workers have concluded that clastic muds rich in terrestrial organic matter and highly organic sapropels accumulated on the floor of the eastern Mediterranean during times of very high Nile flow (Lourens et al., 1996; Cramp and O'Sullivan, 1999; Mercone et al., 2001; Krom et al., 2002; Larrasoaña et al., 2003; Ducassou et al., 2008, 2009; Rohling et al., 2009; Revel et al., 2010; Zhao et al., 2011, 2012; Hennekam et al., 2014).

All of these studies imply that discharge from the Nile was unusually high in order for the sapropels to form, but because they are based on analysis of marine sediment cores from the Nile cone and eastern Mediterranean, they cannot provide direct and independently dated evidence of exceptional floods in the Blue and White Nile catchments during times of sapropel formation. The aim of this paper is to rectify this omission and to provide directly dated sedimentary evidence to show that phases characterized by extreme flood events in the Blue and White Nile catchments were indeed synchronous with sapropel formation in the eastern Mediterranean during the last 125 kyr. We also provide evidence for the first time that three episodes of source-bordering dune formation during the last 115 kyr coincided with times of high flow in the former distributary channels of the Blue Nile that traversed the Gezira alluvial fan (Fig. 1b). Our data come from Pleistocene and Holocene alluvium and sand dunes in our southern study area and Holocene alluvium and wind-blown dust in our northern study area. The lower White and Blue Nile valleys in central Sudan comprise the southern study area (Fig. 1b), and the main or desert Nile valley in northern Sudan to the west and east of Dongola forms the northern study area (Figs. 1a and 6).

2. The southern study area

2.1. The Gezira alluvial fan

The area between the lower Blue and White Nile valleys (Plate 1) is called the *Gezira* (Arabic for island) and is the region we have studied in greatest detail since it provides much of the best-dated evidence of extreme flood phases during the Quaternary. The

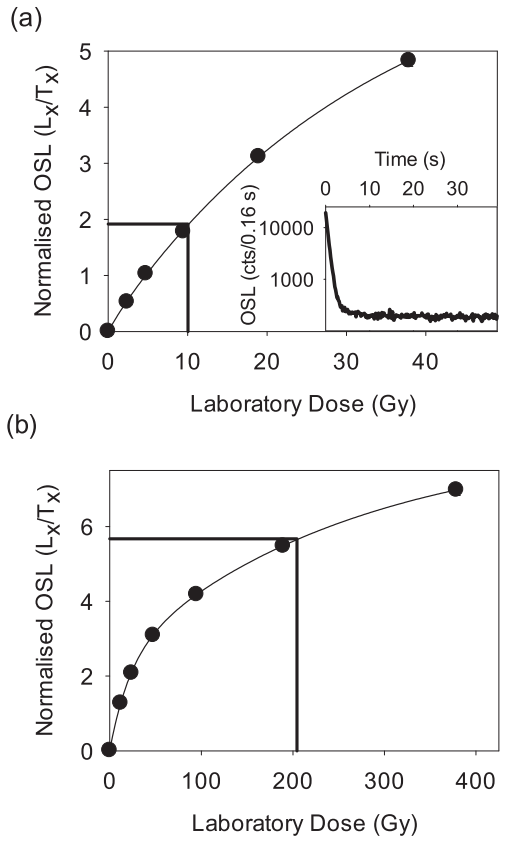

Fig. 2. a. Dose response curve for one aliquot of sample S11/A2-2, which gives a D_e of 10.1 ± 0.3 Gy. The natural OSL decay curve is shown in the inset. Note the logarithmic scale on the y-axis. b. Dose response curve for sample S11/2-3, illustrating the curvature of the OSL response at high doses.

Gezira is a low-angle alluvial fan bounded to the east by the present Blue Nile, to the west by the White Nile and to the south by the Managil Ridge. The Gezira is traversed by a series of defunct sandy channels that originate between the towns of Sennar and Wad Medani on the present-day Blue Nile (Fig. 1b). The sandy channels are unsuitable for irrigation, and are mostly avoided by farmers but are sometimes used as settlement sites for small villages. In addition, sand dunes occupy 150,000 ha of the northwest Gezira, many of them recently reactivated as a result of overgrazing by sheep and goats of the former grass cover (mostly *Panicum turgidum* tussock grass) and removal of trees like *Acacia (*now *Vachellia) tortilis* and *Capparis decidua* for fuel and house building. At shallow depths along the White Nile there are localised areas with very high levels of salinity, which reflect the alluvial history of that river.

2.2. Previous work

Tothill (1946, 1948) was the first to show that the Gezira clays were alluvial and had not been formed by wind-blown dust. He considered that they had been laid down in late Pleistocene and early Holocene times as a result of seasonal flooding from the Blue Nile. He based his conclusions on the presence of aquatic gastropods in the upper 2 m of Gezira clay west of the present Blue Nile and upon the presence of pyroxene and other heavy minerals indicative of a volcanic (i.e., Ethiopian) provenance.

Williams (1966) provided the first radiocarbon ages for two sites east of the White Nile showing that these White Nile alluvial clays had been deposited during the terminal Pleistocene and early Holocene. He also proposed that the Gezira clays had been deposited by seasonal floods from distributary channels of the Blue Nile that radiated across the Gezira alluvial fan. Later work by Williams (1968a) showed that patterns of soil salinity in the western Gezira did not reflect present-day climatic gradients but did reflect the depositional history of the parent sediments. In addition, the hydraulic conductivity of the clays was strongly influenced by soil salinity and alkalinity (Williams, 1968b). The soil catena associated with the dune complex indicated that the dunes were often polygenic and that bodies of standing water had previously occupied the swales between dunes, leaving behind massive beds of calcium carbonate (Williams, 1968c).

Williams and Adamson (1974, 1980, 1982), Adamson et al. (1980, 1982) and Williams et al. (1982, 2000, 2010) conducted a comprehensive programme of radiocarbon dating of gastropod and other shells from Blue and White Nile alluvium and were able to show that there had been a series of Holocene phases of diminishing high flood levels in both rivers, with the last significant moist phase associated with a unique form of pottery manufacture using the siliceous spicules of the swamp dwelling sponge *Eunapius nitens* as temper (Adamson et al., 1987). The dated shells were tested for re-crystallisation using X-ray diffraction and modern Blue and White Nile shells from different species were dated to see if there was any significant reservoir effect. There was not.

The first attempt at luminescence dating of White Nile sediments was on cores collected from a 6 m deep trench dug near the village of Esh Shawal (Fig. 1b) located 265 km upstream from the Blue and White Nile confluence at Khartoum. The OSL ages revealed that White Nile alluvium at this site dated back to at least 240 kyr (Williams et al., 2003), consistent with independent but similar estimates for the approximate age of inception of Lake Victoria in the Ugandan headwaters (Talbot and Williams, 2009; Williams and Talbot, 2009).

Talbot et al. (2000) and Williams et al. (2006) showed that widespread terminal Pleistocene and early Holocene flooding and clay deposition in the lower White Nile valley followed the abrupt return of the summer monsoon in the Ugandan headwaters of the White Nile ~14.5 kyr ago. It also coincided with a sharp decrease in Saharan dust flux into the Atlantic and the onset of what deMenocal et al. (2000) termed the African Humid Period. [This term is in fact a misnomer, since many regions of Africa south of the equator remained dry at this time (Gasse et al., 2008)]. This major Nile flood event caused erosion of many of the sand dunes in the lower White Nile valley (Williams, 2009) and was followed by Blue and White Nile incision and progressively reduced flooding until aridity set in about 4.5 kyr ago (Williams et al., 2010). The sudden return of the summer monsoon was synchronous with abrupt deglacial warming, itself preceded by a synchronization of North Pacific and Greenland climates 15.5 kyr ago, which lasted until 11 kyr ago (Praetorius and Mix, 2014).

Over a century ago Willcocks (1904, p. 42) observed that the Blue Nile flood caused the White Nile to form a seasonal lake for up to 300 km upstream of its present confluence with the Blue Nile at 15°36′ N and 3 km wide at its northern end. Barrows et al. (2014) built upon this observation and obtained ^{10}Be ages for the beach ridge of the last interglacial White Nile when it formed a seasonal lake at least 650 km long and up to 80 km wide, with an area of approximately 45,000 km^2, as a result of a sustained phase of extreme Blue Nile floods at that time. Williams et al. (2003) had previously mapped part of this lake but had not been able to date the beach ridge directly.

Although these investigations have added much extra detail to our knowledge of the Quaternary history of the Nile, three important questions were still unresolved, namely, the age of the Gezira clay, the age of the Gezira palaeochannels, and the age of

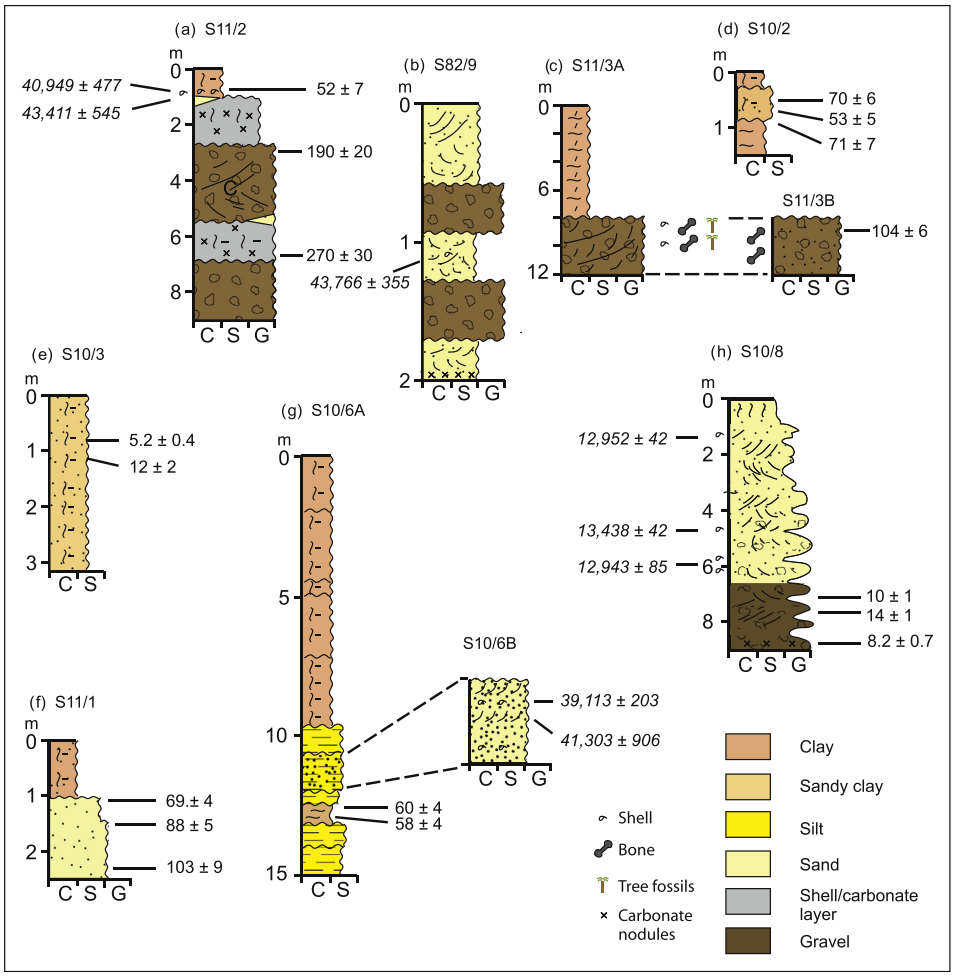

Fig. 3. Stratigraphic alluvial sections of the Quaternary White Nile, Blue Nile and Dinder Rivers, central Sudan.

the lower White Nile dune complex. Our fieldwork in February 2010 and January–February 2011 has helped to provide some firm numerical ages in answer to these questions, and has shown that phases of extreme Nile floods have been synchronous with times of sapropel accumulation in the eastern Mediterranean during the past 125 kyr.

3. The northern study area

3.1. The Northern Dongola Reach

Most of the work on the Holocene alluvial record of northern Sudan has been carried out in an 80 km segment of the Northern Dongola Reach (NDR), which contains the New Kingdom site of Kawa (Fig. 6b). This is a low gradient alluvial reach upstream of the Third Cataract underlain by Nubian Sandstone and bordered to the east by a well-defined bedrock plateau. The maximum distance from the modern river to the plateau is about 18 km. In general, there is very little relief between the plateau and the modern river corridor except where belts of sand dunes are found. A few kilometres north of Kawa, river flows have been recorded at Dongola for over a century. Upstream of this town the Nile catchment extends over 1.6 million km^2. Research on the Holocene river history of the NDR was stimulated by, and carried out in collaboration with, a long-term exploration of the archaeology of the valley floor (Welsby et al., 2002).

3.2. Previous work

The Holocene archaeology provides important insights into the long-term behaviour of the Nile in this part of the catchment. The archaeological record was surveyed in detail in the mid-1990s by the Sudan Archaeological Society (SARS) led by Derek Welsby of The British Museum (Welsby, 2001; Welsby et al., 2002). This project recorded more than 450 archaeological sites between the modern Nile and the bedrock plateau – the vast majority of these sites date to the Neolithic (before 3500 BC) and Kerma periods (2400 BC to 1450 BC). The SARS survey identified three major palaeochannel belts and named them the Hawawiya Nile and Alfreda Nile – these channel belts converge in the northern part of the study area to form the Seleim Nile (Welsby et al., 2002; Woodward et al., 2001), which flowed all the way to Kerma (55 km to the north) throughout the Neolithic and Kerma periods. The modern course of the river is known as the Dongola Nile.

A key aim of the geomorphological research was to develop a robust independent dating framework for river activity in the NDR and to work closely with the SARS team to explore the long-term relationship between Holocene river dynamics and human activity (Woodward et al., 2001; Macklin et al., 2013). A further aim was to establish the wider significance of this river history within and beyond the Nile basin.

Since the first geomorphological field season in 1995, a large body of data has been assembled on the Holocene alluvial record in the NDR from field mapping and via sections exposed in

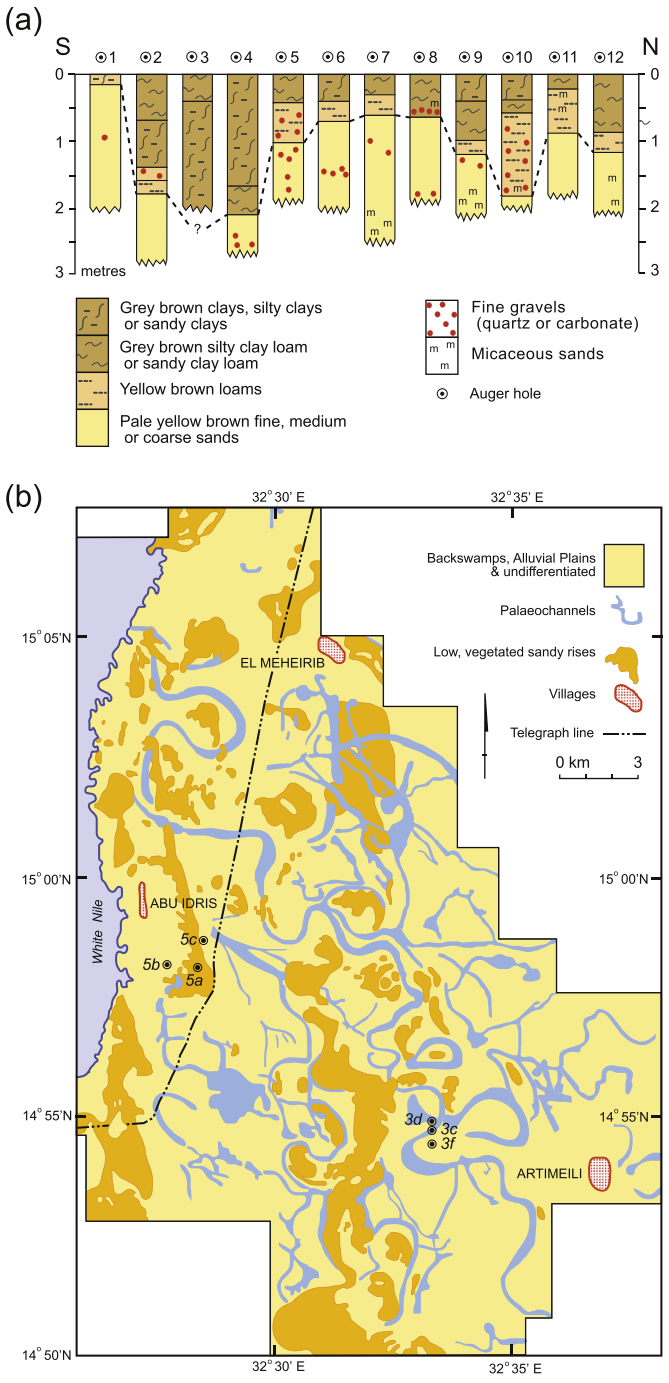

Fig. 4. a. Blue Nile palaeochannel meanders east of the lower White Nile near El Geteina (after Williams, 2009) showing location of certain dated stratigraphic sections. b. Stratigraphic section across a palaeochannel meander 7 km west of Artimeili village showing fining upward sequence from late Pleistocene to Holocene (after Williams, 2009).

groundwater pump pits, archaeological excavations and ancient well shafts (Woodward et al., 2001; Welsby et al., 2002; Williams et al., 2010; Macklin et al., 2013). A dating framework has been created based primarily on OSL dating of sand units with a smaller number of radiocarbon dates on charcoal associated with *in situ* archaeological features. This is one of the best-dated Holocene fluvial records in the desert Nile (see Macklin et al., 2013 for details). The sites marked in black and red on Fig. 6a indicate the locations to the east of the modern Nile where the fluvial record has been dated by OSL or ^{14}C as reported in Macklin et al. (2013).

About 15 km west of the main Nile in the NDR, Williams et al. (2010) have reported radiocarbon ages from diatomaceous lacustrine silts deposited in the Qaab Depresssion. During periods of very high Nile flows, this former lake basin was fed by an east–west aligned overflow channel that exited the main Nile on latitude 19°37′N. Three calibrated radiocarbon assays from freshwater gastropod shells bracket a phase of early to early-mid Holocene lacustrine sedimentation in the basin (10,073 ± 96, 7862 ± 45 and 7431 ± 54 cal yr BP: see Williams et al., 2010, Table 4).

4. Optically stimulated luminescence dating procedures

Optically stimulated luminescence dating was applied to a suite of samples to determine the age of sediment deposition. Samples were collected from freshly cleaned sedimentary faces by hammering opaque tubes into the surface. The tubes were sealed to prevent light exposure at each end, and then returned to the luminescence laboratory where further analysis was undertaken under subdued red lighting. Two laboratories undertook analysis, one at the University of Adelaide and one at Aberystwyth University. The two laboratories used similar analytical procedures, and the data sets produced have previously been shown to be comparable (Macklin et al., 2013).

The environmental dose rate to the grains was determined using a sub-sample of the material collected for luminescence measurements. After drying, the samples were finely milled and homogenised. A variety of methods were used for dosimetry. In Aberystwyth the beta dose rate was measured directly using a GM-25-5 beta counter, and the gamma dose rate calculated from ICP-OES and ICP-MS measurements of K, U and Th. In Adelaide the chemical composition of the sediments was also measured, using ICP-AES and ICP-MS. Additional measurements of U and Th were made using thick source alpha counting, and of K using X-ray fluorescence spectroscopy. The cosmic dose rate for all samples was calculated using the relationship between cosmic ray penetration, depth and latitude (Prescott and Hutton, 1994). Where multiple methods of dose rate determination were undertaken, the results were averaged. The dose rates were corrected for the effect of grain size and water content, and are given in Table 1.

Samples for luminescence measurements were chemically treated with HCl and H_2O_2 to remove carbonates and organics, dry sieved to obtain grains in a narrow size range, density separated (2.62–2.70 g/cm^3), etched in hydrofluoric acid to remove feldspars and etch the outer surface of the grains, and were finally sieved again to remove any residual feldspar fragments. This pure quartz fraction was then used for luminescence measurement using blue LEDs to generate an OSL signal. The single aliquot regenerative dose (SAR) procedure was used to determine the equivalent dose (D_e), and 24 aliquots were measured for each sample to assess the reproducibility of the D_e. Data were screened using five acceptance criteria: (1) a recycling ratio within 10% of unity (15% for samples analysed in Adelaide), (2) and IR OSL depletion ratio (Duller, 2003) within 10% of unity (15% for samples analysed in Adelaide), (3) a net OSL signal from the first test dose that is at least three times greater than the standard deviation of the background, (4) a dose response curve that increases monotonically, and (5) recuperation, as measured for the zero dose point, that is less than 15% of the natural signal. These screening criteria tended to only remove 2–4 aliquots from each dataset (Table 1).

A number of different types of sediment was analysed including eolian sands blown into palaeochannels, dune sands and channel fills. An objective approach based on calculation of the over-dispersion (OD) of the D_e distribution was taken to assess whether the distribution of equivalent dose values was consistent with complete removal of trapped charge at the time of deposition. The OD of the dataset expresses the scatter in the dataset beyond that which can be explained by the measurement uncertainties.

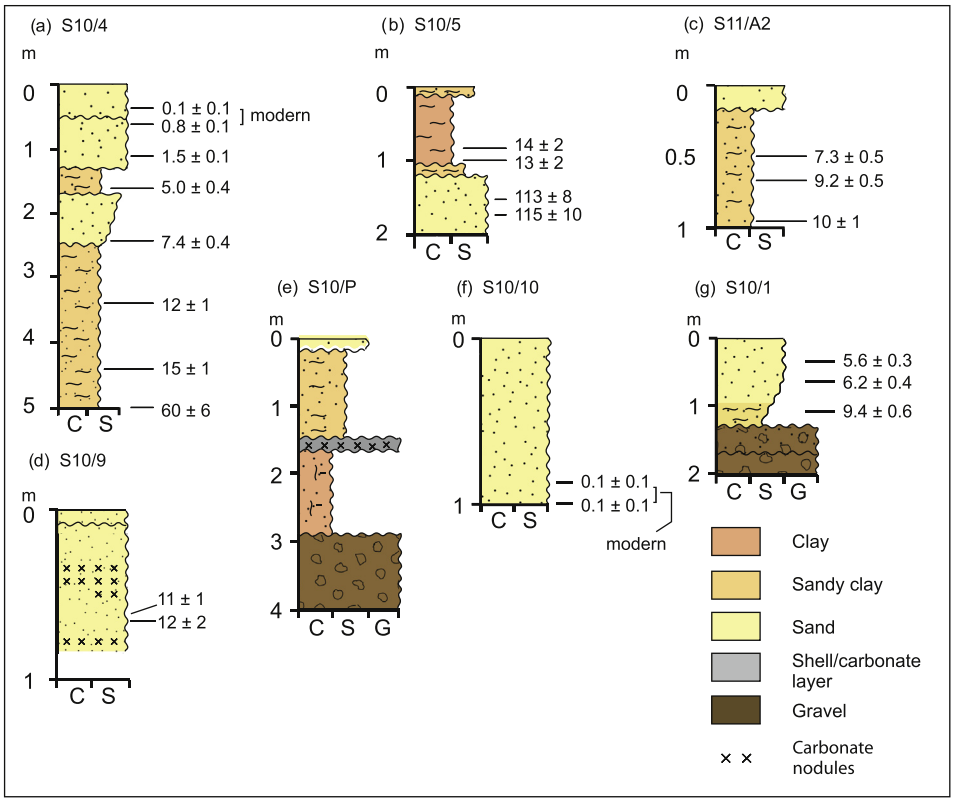

Fig. 5. Stratigraphic sections through Late Quaternary sand dunes, lower White Nile valley, central Sudan, and west of 6th Cataract, Sabaloka gorge, Main Nile valley.

Where the OD was less than 20% the datasets were considered to be well bleached and the central age model (CAM) (Galbraith et al., 1999) was applied to the dataset. If the OD was greater than 20% then the finite mixture model (FMM) (Galbraith and Green, 1990) was applied to identify the best bleached component following the method of Rodnight et al. (2006). In general, where the FMM was applied, 90% of more of the D_e values were in the best bleached component, suggesting that if any incomplete bleaching occurred, it was limited in its impact. The age of each sample was calculated by dividing the D_e by the dose rate (Table 1).

The OSL signal from quartz in these samples was generally bright and dominated by a fast component (inset to Fig. 2a), and the suitability of the SAR protocol for measurement of these samples is demonstrated by the high proportion of aliquots that passed the screening criterion. The majority of samples analysed in this study yielded D_e values that are comfortably within the range of the OSL dose response curve (Fig. 2a), and their reliability is supported by comparisons of quartz OSL ages with independent age control (Murray and Olley, 2002). A number of the samples were older, with equivalent dose values of 100 Gy or higher. In these samples the impact of saturation of the OSL signal is clear (Fig. 2b). Whilst the reliability of older OSL ages continues to be debated, these samples have natural signals that are less than 85% of the fully saturated value that Wintle and Murray (2006) suggested may be the upper limit for OSL dating, and ages are in stratigraphic order within uncertainties.

5. Quaternary environments in the lower Blue and White Nile valleys

5.1. Age of the Gezira clay

Williams and Adamson (1980, 1982) suspected that the surface of the Gezira clay plain was diachronous. However, they were unable to provide firm evidence in support of this hypothesis, beyond noting that at Soba on the Blue Nile just upstream from Khartoum the radiocarbon ages of massive laminated carbonates along the banks of the Blue Nile showed them to be of late Pleistocene age. In addition, the surface grey clay unit when traced laterally for 15 km east of Esh Shawal was found to be underlain by a massive brown clay containing recrystallised gastropod shells of unknown age but certainly older than 15 kyr (Williams et al., 1982).

In February 2011 we sampled *Etheria elliptica* (Nile oyster) shells in the base of a surface grey clay unit 1–5 m thick exposed in the gravel quarries south of El Masoudia (Fig. 1b) located about 0.5 km west of the Blue Nile at 15°18′ N and 32°53′ E. The oyster shells had calibrated AMS ^{14}C ages of 40, 949 ± 477 and 43,411 ± 545 (Table 2) and the OSL age near the base of the grey clay was 52 ± 7 kyr (Table 1; Fig. 3: site 3a). We can draw several conclusions from these new ages. First, the uppermost clay layer in the Gezira ranges in age from Holocene to at least 40–50 kyr. It follows from this that certain portions of the Gezira alluvial fan have been inactive since the late Pleistocene while others have received sediment until early to middle Holocene times.

5.2. Age of the Gezira, Blue Nile and Dinder palaeochannels

A series of planar and cross-bedded fluvial sandy gravel units are clearly exposed beneath the 40–50 kyr surface clay unit in the Masoudia gravel quarries (Fig. 3: site 3a). Sand lenses in two of the lower units have yielded OSL ages of 270 ± 30 kyr and 190 ± 20 kyr (Table 1). A long interval of soil development followed the deposition of the older of the two Blue Nile gravel units visible in the quarries, and gave way to renewed gravel deposition and a further interval of prolonged pedogenesis and precipitation of irregular carbonate nodules and rhizocretions, under a climate that was probably as dry as that of today. A minor phase of erosion ensued, with deposition of rolled and well rounded carbonate gravels,

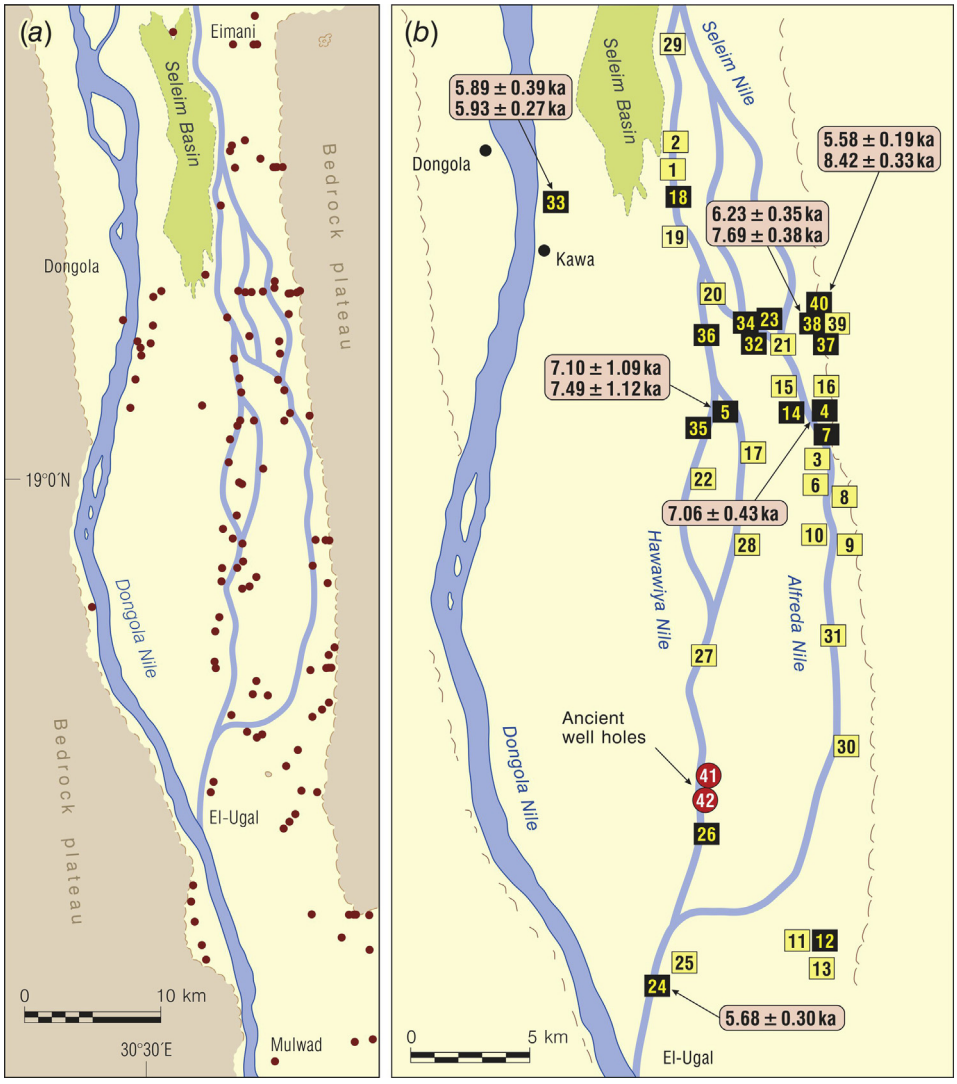

Fig. 6. a. The Dongola Reach of the present-day Nile and the palaeochannel belts in the Northern Dongola Reach, showing the distribution of Neolithic sites. b. Locations where we have logged sections and/or dated samples from the Holocene alluvial record.

presumably derived from erosion of the underlying calcareous palaeosol, and this was in turn followed by deposition of the surface grey clay mantle 40–50 kyr ago, with Nile oysters concentrated in the lower 10–15 cm of the clay. The alluvial clays indicate widespread flooding as a result of a stronger summer monsoon in the Ethiopian headwaters of the Blue Nile at this time. The early stages of such flood events would have caused death by mass burial of beds of Nile oyster (*Etheria elliptica*) as a result of a sudden influx of abundant fine sediments, much as in the Roseires Dam reservoir today (Wohl, 2011, p. 80). The oysters' preferred habitat is a rocky substrate and they are tolerant of fast flow, but die if smothered in fine sediment. Across the Gezira three gravel pits located 2 km north of Naima just east of the White Nile (Fig. 1b) revealed up to 2 m of alluvial gravels with oyster shells, one of which yielded an AMS ^{14}C age of 38,900 ± 350 ^{14}C yr BP and a calibrated age of 43,766 ± 355 cal yr BP (Table 2; Fig. 3, site 3b). These pits were located near the distal end of a Blue Nile palaeochannel (Fig. 1b).

We examined two fossil-bearing sites near the village of Branko (Fig. 1b) at 14°58′N and 33°15′E on the east bank of the Blue Nile ~150 km upstream from its confluence with the White Nile (Fig. 3: site 3c). One site was located ~1 km north of the village, and the other ~2 km south of the village. The southern site had previously yielded silicified bones of what is probably a rhinoceros femur (Dr Leslea Hlusko, University of California, Berkeley, *in litt*., January 2011; Dr Veerle Linseele, University of Louvain, spoken confirmation, January 2011) (Plate 2) embedded in partially cemented cross-bedded coarse fluvial sands and fine gravels, for which we obtained an OSL age of 104 ± 6 kyr (Table 1; Fig. 3: site 3c). The northern site belongs to the same stratigraphic unit and so is of similar age. It contained three broken pieces of a fossilised tree trunk 0.6–1.0 m in diameter and 4.05 m long, entirely replaced by crystalline calcium carbonate. From its dimensions, the tree may have been a former riparian *Acacia (*now *Senegalia) senegal* or one of the big deciduous trees such as *Combretum* that today grow over 300 km further south. There were also abundant silicified fragmentary mammal bones, horn cores and Nile oyster shells (*Etheria elliptica*) embedded in carbonate-cemented fluvial coarse sands and gravels. We also observed a fossil branch 26 cm long and 3.5 cm diameter entirely encircled by a fossilised liana, suggesting a possible rain forest provenance. The gravels form a low terrace that is flooded during the summer rainy season but preserved from erosion by strong carbonate cementation (Barrows et al., 2014).

A series of sinuous palaeochannels are very clearly visible on air photographs of the northwest Gezira (Fig. 4a; Plate 3). These channels continue towards the White Nile and disappear beneath the dunes located between Jebel Aulia in the north and Naima in

Fig. 7. Blue Nile headwaters. Land over 2000 m is shown in brown. Note location of stratigraphic section 3 g on the banks of the Dinder.

the south (Fig. 1b). In January 2010, we sampled two soil pits located 7 km west of Artimeili village at 14°54′ N and 32°33′ E. One pit was situated in a former back swamp, and had OSL ages of 70 ± 6 kyr, 53 ± 5 kyr and 71 ± 7 kyr (Table 1) at depths between 0.4 and 0.8 m below the surface (Fig. 4a: site 3d). Scattered across the surface were very hard rhizocretions of recrystallised calcium carbonate and fragments of fossil bone and, possibly, petrified wood.

A second soil pit located ~400 m south of the 76–50 kyr back swamp pit was in the centre of a large meandering palaeochannel. The channel consisted of very hard dark grey-brown sandy clay to a depth of at least 3.35 m. One clay sample at 85 cm depth gave an OSL age of 5.2 ± 0.4 kyr while another from 112 cm depth had an OSL age of 12 ± 2 kyr (Fig. 1b; Fig. 3: site 3e). These ages are surprisingly young and may simply denote seasonal flooding from the Blue Nile during the early to mid-Holocene, blanketing pre-existing landforms in a veneer of clay. Alternatively, the palaeochannel continued to function until that time, with the clay denoting its final phase of activity.

We returned to this site in February 2011 and after some initial augering located a thinner portion of the dark grey brown sandy clay mantle, which was underlain by sand below a depth of 105 cm, similar to the palaeochannel stratigraphy recorded by Williams (2009) in which up to 1.5 m of dark grey clay was underlain by alluvial sands and fine rounded gravels (Fig. 4b). The sand at this site varied from fine to medium loamy sand with traces of mica and became browner with depth. Three samples gave OSL ages of 69 ± 4 kyr at 111–120 cm depth, 88 ± 5 kyr at 146–156 cm depth, and 103 ± 9 kyr at 232–242 cm depth (Table 1; Fig. 3: site 3f). These ages are very consistent stratigraphically and indicate a prolonged phase of fluvial sand entrainment and deposition in this area between about 100 kyr and 70 kyr ago. The overlap in age with the 70–50 kyr back swamp sediments suggests that they may have belonged to the same drainage system, which remained intermittently active for ~50 kyr in this locality.

The Dinder is a major Ethiopian tributary of the Blue Nile (Figs. 1b and 7). We collected three OSL samples of horizontally-bedded fluvial fine sandy clays and silts from the base of the 15 m high right bank of the Dinder near the village of Azaza Damos at 12°57′ N and 34°38′ E, within sight of the Ethiopian escarpment to the east. The upper 10 m of the section consist of grey brown vertisolic clays. The two lower silty units gave OSL ages of 58 ± 4 kyr and 60 ± 4 kyr (Table 1; Fig. 3: site 3g). A shell-bearing section located 150 m to the south and within the same stratigraphic unit gave calibrated AMS ^{14}C ages for the gastropod and mussel shells of 41,303 ± 906 cal yr BP and 39,113 ± 203 cal yr BP, with one sample giving an AMS ^{14}C age of 47, 814 ± 412 ^{14}C yr BP (Table 2; Fig. 3: site 3g) outside the present calibration range.

These ages are similar to the calibrated AMS ^{14}C ages of 40, 949 ± 477 and 43,411 ± 545 (Table 2; Fig. 3: site 3a) for the *Etheria elliptica* Nile oyster shells collected from the base of the grey clay at the Masoudia gravel quarry 500 m from the left bank of the modern Blue Nile (Fig. 4a). The ages are also very similar to the calibrated AMS ^{14}C age of 43,766 ± 355 yr BP for oyster shells from alluvial gravels near the distal end of a Blue Nile palaeochannel located 2 km north of Naima just east of the White Nile (Fig. 1b). Our tentative interpretation is that these ages mark the closing stages of a regime characterised by the transport of coarser sediment by the late Pleistocene Dinder and Blue Nile rivers, and its replacement with a suspension load regime of silt and clay.

An informative Blue Nile palaeochannel section (Plate 4) was afforded by the Blue Nile sand quarry north of Singa (Fig. 1b) at 13°16.5′ N and 33°43′ E. The channel sands in this section appear to have been deposited during the early to mid-Holocene. Shells collected at depths of −1.7 m, −4.7 m and −6.0 m from the upper surface of the quarry yielded calibrated AMS ^{14}C ages of 12, 952 ± 42, 13, 438 ± 42 and 12, 943 ± 85 cal yr BP, respectively (Table 2; Fig. 3: site 3h). Three sand samples from depths of −8.8 m, −7.75 m and −7.25 m had OSL ages, respectively, of 8.2 ± 0.7 kyr, 14 ± 1 kyr and 10 ± 1 kyr (Table 1; Fig. 3: site 3h), which are somewhat younger than the shell radiocarbon ages. The terminal Pleistocene around 14.5 kyr marked the return of the summer monsoon with renewed seasonal flood flows in the Blue and White Nile rivers (Talbot et al., 2000; Williams et al., 2003, 2006; Marshall et al., 2011).

We are now in a position to summarise what is presently known about the age and abandonment of the Gezira and Blue Nile palaeochannels. The late Quaternary channels that radiate across the Gezira carried a bed load of sand and fine gravel from the volcanic uplands of Ethiopia. The heavy mineral suite of the source-bordering dunes and sandy point-bars associated with these channels is virtually identical to the heavy mineral assemblage from Blue Nile channel sands collected by one of us (MAJW) in December 1971 from the bottom of the Blue Nile gorge near Dejen in the highlands of Ethiopia (Williams and Adamson, 1973) and to the Blue Nile heavy mineral suite described in detail by Garazanti et al. (2006) and Garzanti (this volume). In order of abundance, the most common minerals in the Blue Nile gorge bedload sample are volcanic rock fragments, quartz, magnetite, plagioclase, pyroxene, epidote, hornblende, rutile and zircon. The quartz grains in the Blue Nile sediment come from the Triassic Adigrat Sandstones exposed at the base of the cliffs in the gorge as well as from the granites that crop out over 100 km downstream. The most common minerals in the dune sands are quartz, plagioclase, biotite, hornblende, magnetite, pyroxene, epidote, rutile, microline, feldspar, calcite, limonite and zircon. Basalt fragments were also common in some dunes.

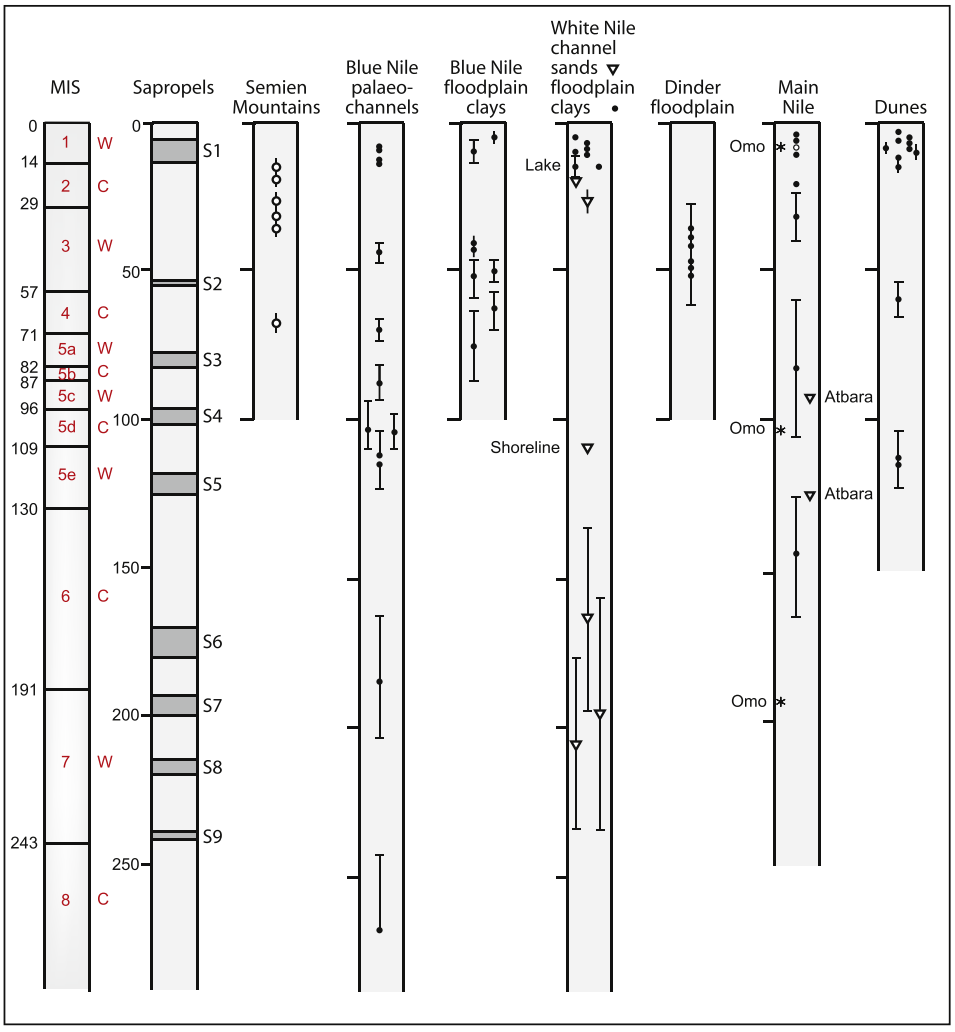

Fig. 8. Phases of high Nile floods in relation to dated intervals of sapropel formation in the East Mediterranean during the last 250 kyr.

Radiocarbon dates obtained previously on oyster and gastropod shells, charcoal and carbonate samples within the palaeochannel sediments suggested that the Blue Nile palaeochannels were at least seasonally active between >40 kyr and about 5 kyr (Williams, 2009). The present work has extended the age of these surface channels back to at least 100 kyr and the near surface channels to at least 270 kyr (Masoudia gravel quarry site). The abandonment of the surface channels was a direct result of Holocene incision by the main Blue Nile channel, which began at least 8 kyr ago (Arkell, 1949, 1953; Adamson et al., 1982; Williams et al., 1982; Williams et al., this volume). This incision effectively beheaded the distributary channels and deprived them progressively of their flood discharge. As the Nile cut down into its former floodplain, a series of shallow drainage channels remained seasonally active and finally dried out.

The final stages of infilling of these palaeochannels and adjacent floodplains involved deposition of a thin layer of dark grey-brown clay. The fining-upwards sequence reflects a change from the transport of pale yellow medium and coarse quartz sands and fine quartz and carbonate gravels derived from hard pedogenic nodules to grey brown silty clays, sandy clays and clays in the upper 50–150 cm. Clay deposition in the back swamps and flood plains of these channels dwindled and finally ceased about 5 kyr ago, when the seasonally flooded swampy plains gave way first to acacia – tall grass savanna and finally to semi-desert steppe. The fossil snail fauna within the upper 2 m of Holocene Gezira clay shows a progressive change from permanent water species such as *Melanoides tuberculata*, *Bulinus truncatus*, *Biomphalaria pfeifferi* and *Cleopatra bulimoides* to semi-aquatic species with lungs and gills (*Lanistes carinatus*, *Pila wernei*) to land snails (Tothill, 1946, 1948; Williams et al., 1982). One of these, the large land snail *Limicolaria flammata*, today inhabits the acacia – tall grass savanna region to the south of Sennar (Fig. 1b) where the annual rainfall is at least 450–500 mm, in contrast to the 175 mm that now falls at Khartoum. *Limicolaria* was at its most widespread in this region ~5.2 kyr ago.

5.3. Age of the lower White Nile dune complex

As noted in Section 5.2, analysis of the heavy mineral assemblage in the upper 3 m of the sand dunes located on a 100 km north to south transect immediately east of the present White Nile is consistent with an ultimate sediment source in the Ethiopian headwaters of the Blue Nile. These dunes may therefore be considered as source bordering dunes blown from sandy point bars fed by a regular supply of Blue Nile sand until the Gezira palaeochannels ceased to flow in the early to mid-Holocene.

Three conditions are necessary for the formation of source-bordering dunes (Williams, 2014, pp. 120–121). The first

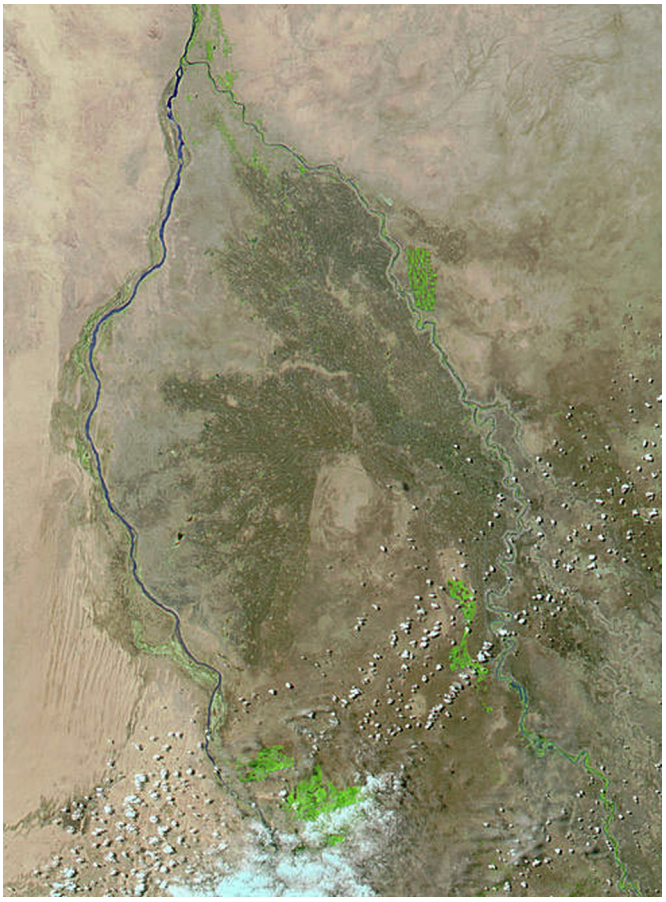

Plate 1. Satellite image showing the area between the lower Blue and White Nile on June 19, 2003 (compare Fig. 1b). The image is from the Moderate Resolution Imaging Spectroradiometer (MODIS) Aqua satellite, courtesy Jacques Descloitres, MODIS Rapid Response Team at NASA GSFC. Gezira Irrigation Area appears brown on this image. The top of the image is north. The distance from south to north is 320 km.

prerequisite is a regular supply of bed-load sands brought in by rivers that dry out seasonally, leaving their sandy point-bars exposed to deflation. The second requirement is an absence of riparian vegetation so that sand movement out of the channel through deflation is not impeded. The third condition is a regime of strong unidirectional winds to allow the mobilisation and transport of sand from the dry river channel to form linear dunes downwind of the channel. In regard to the first condition, for the dunes to develop and continue to extend downwind, the alluvial sand supply needs to be regularly replenished. Once the sand supply eventually ceases, the dunes would become vegetated and relatively stable. If this analysis is correct, then any ages obtained for phases of dune accretion need not be indicative of aridity but could simply denote changes in sand supply, wind speed and dune surface plant cover.

A pit was dug on the summit of a prominent N–S aligned 9 m high vegetated linear dune (Plate 5) located ~2.5 km east of and parallel to the right bank of the White Nile at 14°58.5′ N and 32°28′ E (Fig. 4a). Along the western flanks of this dune were recently exposed human skeletons associated with charcoal, ostrich eggshell fragments and freshwater mussel shells, with calibrated ^{14}C ages between 3 and 1 cal kyr BP (Table 2, site 11/4, close to site 5b on Fig. 4a). The dune pit was 1.8 m deep and was extended a further 3.25 m by hand auger, giving a total depth of 5.05 m (Fig. 5: site 5a). The upper 1.8 m of the pit consisted of fine well-sorted eolian sand with OSL ages increasing from 0.8 ± 0.1 kyr at −0.6 m, to 1.5 ± 0.1 kyr at −1.1 m, to 5 ± 0.4 kyr at −1.75 m (Table 1). Below that level the sand changed progressively from a brown sandy clay loam at −2 m to a sandy clay at −4.4 m, becoming calcareous below that depth, with up to 20% irregular calcium carbonate nodules. The OSL ages were 7.4 ± 0.4 kyr at −2.4 m, 12 ± 1 kyr at −3.4 m, 15 ± 1 kyr at −4.4 m and 60 ± 6 kyr at −5 m. The texture changed abruptly to a massive fine sandy loam at a depth of 4.55–4.70 m, suggestive of a change in depositional regime or an interval of soil formation. The sudden jump in age from ~15 kyr at −4.4 m to ~60 kyr at −5 m suggests that there may have been one or more phases of erosion and/or non-deposition, stabilisation and pedogenesis at some stage between 60 and 15 kyr.

A second pit excavated on the gently sloping floodplain ~1.4 km west of the base of the dune gave some interesting results (Fig. 4; Fig. 5: site 5b). Calcareous silty clay at a depth of 83–93 cm had an OSL age of 14 ± 2 kyr and an age of 13 ± 2 kyr at 98–103 cm depth, both ages overlapping at one standard deviation from the mean. Below 107 cm depth the overlying clay gave rise to very well sorted very fine sand that we very tentatively consider to be of wind-blown origin, although a fluvial origin cannot be ruled out. The fine sand at 147–157 cm depth has an OSL age of 113 ± 8 kyr, and that at 160–170 cm depth an OSL age of 115 ± 10 kyr (Table 1). These last two ages are broadly similar to that of 103 ± 9 kyr for the fine fluvial sand at 232–242 cm depth in the Artimeili palaeochannel site (Table 1) in the north–central Gezira (Fig. 4; Fig. 3: site 3f). That particular palaeochannel can be traced laterally northwest on aerial photographs until it runs beneath the linear dune on its path towards the White Nile (Fig. 4a). The two sands may even belong to the same palaeochannel complex, but further speculation seems unwarranted.

We were able to obtain three OSL ages for the grey sandy clays immediately east of the visible base of the 9 m dune (Fig. 5: site 5c). The clays were overlain by 35 cm of red brown clayey sand. The OSL ages were 7.3 ± 0.5 kyr at 57–70 cm depth, 9.2 ± 0.5 kyr at 70–80 cm depth, and 10.0 ± 1 kyr at 94–102 cm depth (Table 1), all consistent with Holocene flooding and clay deposition.

A degraded dune 1.5 km northeast of El Geteina (Fig. 1b) at 14°52.6′ N and 32°23.4′E revealed the following depositional sequence (Fig. 5: site 5d), from the surface down: (a) 0–17 cm: dry loose single grain reddish-yellow wind blown medium sand, with a sharp clear boundary to underlying unit. (b) 17–55 cm: loamy medium sand with a weak coarse sub-angular blocky structure and soft white calcium carbonate below 35 cm. (c) 55–70 cm: massive sandy clay loam with 3–5% soft diffuse calcium carbonate. The OSL age at 60 cm depth was 11 ± 1 kyr and at 66 cm depth was 12 ± 2 kyr (Table 1). (d) 70–84 cm: massive light sandy clay loam with 50% slightly hard pedogenic calcium carbonate nodules up to 1 cm in size.

A 4 m deep gravel pit opened in January 2010 in connection with the gas pipeline and located at 14°52.6′ N and 32°23.9′E, near to the El Geteina degraded dune pit, proved informative (Fig. 1b; Fig. 5: section 5e), although we were not able to obtain samples for dating. From the surface down the section consisted of four main depositional units: (a) 0–20 cm: loose dry single grain wind-blown sand. (b) 20–150 cm: massive grey brown sandy clay loam grading upwards to sandy loam. (c) 150–280 cm: massive brown sand clay soil with irregular pedogenic calcium carbonate nodules in the upper 25 cm. (d) 280–400 cm: rolled calcium carbonate fluvial gravels.

The following sequence of events may be inferred from the two trenches near El Geteina: (1) deposition of late Pleistocene fluvial gravels; (2) deposition of alluvial clay followed by late Pleistocene pedogenesis and calcium carbonate precipitation within the soil profile; (3) erosion of the soil surface; (4) terminal Pleistocene and early Holocene deposition of wind-blown sand.

A pit 1 m deep was dug on the summit of a low dune ~2 km east of the degraded dune pit at 14°52.5′ N and 32°24.6′E. The dune

Table 1
Optically stimulated luminescence ages for sites in the White Nile, Blue Nile and Dinder valleys, central Sudan. *Denotes age cited in Barrows et al., 2014.

Sample	Section/Fig. no.	Depth (m)	Grain size (μm)	Beta[1]	Gamma[1]	Cosmic	Total	Num. Aliquots	Age Model	De (Gy)	Age (ka)
Dose Rate (Gy/ka)											
S10/1-1 Ad	5g	1.07	125–180	0.41 ± 0.03	0.32 ± 0.05	0.19 ± 0.02	0.92 ± 0.03	22(24)	CAM	8.7 ± 0.5	9.4 ± 0.6
S10/1-2 Ad		0.63	125–180	0.41 ± 0.05	0.31 ± 0.03	0.20 ± 0.02	0.93 ± 0.03	22(24)	FMM	5.7 ± 0.3	6.2 ± 0.4
S10/1-3 Ad		0.33	125–180	0.43 ± 0.03	0.32 ± 0.03	0.20 ± 0.02	0.96 ± 0.03	23(24)	FMM	5.4 ± 0.3	5.6 ± 0.3
S10/2-1 Ad	3d	0.50	125–180	1.08 ± 0.07	0.58 ± 0.03	0.20 ± 0.02	1.86 ± 0.05	24(24)	CAM	131 ± 7	70 ± 6
S10/2-2 Ad		0.70	125–180	0.94 ± 0.06	0.51 ± 0.03	0.19 ± 0.02	1.66 ± 0.04	23(24)	CAM	88 ± 6	53 ± 5
S10/2-3 Ad		0.79	125–180	1.06 ± 0.07	0.58 ± 0.03	0.19 ± 0.02	1.85 ± 0.05	24(24)	CAM	131 ± 9	71 ± 7
S10/3-1 Ad	3c	0.85	125–180	0.82 ± 0.04	0.62 ± 0.03	0.19 ± 0.02	1.64 ± 0.05	24(24)	FMM	8.6 ± 0.5	5.2 ± 0.4
S10/3-2 Ad		1.12	125–180	0.88 ± 0.04	0.68 ± 0.03	0.18 ± 0.02	1.76 ± 0.06	23(24)	FMM	21 ± 4	12 ± 2
S10/4-1 Ad	5a	1.60	125–180	0.52 ± 0.04	0.26 ± 0.02	0.18 ± 0.02	0.96 ± 0.03	23(24)	CAM	4.9 ± 0.3	5.0 ± 0.4
S10/4-2 Ad		1.10	125–180	0.50 ± 0.04	0.25 ± 0.02	0.19 ± 0.02	0.94 ± 0.04	24(24)	FMM	1.4 ± 0.1	1.5 ± 0.1
S10/4-3 Ad		0.60	125–180	0.55 ± 0.04	0.32 ± 0.03	0.20 ± 0.02	1.07 ± 0.03	24(24)	CAM	0.9 ± 0.1	0.8 ± 0.1
S10/4-4 Ad		0.35	125–180	0.48 ± 0.03	0.27 ± 0.02	0.20 ± 0.02	0.96 ± 0.03	32(32)	CAM	0.1 ± 0.1	0.1 ± 0.1
S10/4-6 Ab		2.4	180–212	0.57 ± 0.04	0.29 ± 0.02	0.17 ± 0.02	1.04 ± 0.04	23(24)	CAM	7.7 ± 0.2	7.4 ± 0.4
S10/4-7 Ab		3.4	180–212	0.61 ± 0.04	0.39 ± 0.02	0.14 ± 0.04	1.13 ± 0.06	24(24)	CAM	13 ± 1	12 ± 1
S10/4-8 Ab		4.4	180–212	0.66 ± 0.04	0.38 ± 0.02	0.12 ± 0.03	1.16 ± 0.06	24(24)	CAM	17 ± 1	15 ± 1
S10/4-9 Ab		5.0	180–212	0.77 ± 0.05	0.67 ± 0.04	0.12 ± 0.06	1.56 ± 0.09	24(24)	CAM	93 ± 8	60 ± 6
S10/5-1 Ad	5b	0.87	125–180	0.71 ± 0.05	0.45 ± 0.03	0.19 ± 0.02	1.36 ± 0.04	17(24)	FMM	20 ± 2	14 ± 2
*S10/5-2 Ad		1.00	125–180	0.81 ± 0.05	0.48 ± 0.03	0.19 ± 0.02	1.48 ± 0.04	22(24)	FMM	19 ± 2	13 ± 2
S10/5-3 Ab		1.5	180–212	0.71 ± 0.03	0.36 ± 0.02	0.17 ± 0.02	1.24 ± 0.03	21(24)	CAM	141 ± 10	113 ± 8
S10/5-4 Ab		1.65	180–212	0.85 ± 0.04	0.34 ± 0.01	0.17 ± 0.02	1.36 ± 0.04	24(24)	CAM	156 ± 13	115 ± 10
S10/6-1 Ad	3g	0.50	125–180	1.14 ± 0.08	0.48 ± 0.03	0.20 ± 0.02	1.82 ± 0.05	24(24)	CAM	0.4 ± 0.1	0.2 ± 0.1
S10/6-2 Ad		12	125–180	0.55 ± 0.03	0.30 ± 0.02	0.07 ± 0.01	0.92 ± 0.04	23(24)	n/a	Not datable	
S10/6-3 Ad		12.5	125–180	0.55 ± 0.24	0.30 ± 0.02	0.07 ± 0.01	0.93 ± 0.04	21(24)	CAM	56 ± 3	60 ± 4
S10/6-4 Ad		13	125–180	0.43 ± 0.03	0.28 ± 0.02	0.06 ± 0.01	0.78 ± 0.03	18(24)	FMM	45 ± 3	58 ± 4
S10/8-1 Ad	3h	8.80	125–180	0.96 ± 0.07	0.47 ± 0.03	0.20 ± 0.02	1.63 ± 0.05	24(24)	FMM	13 ± 1	8.2 ± 0.7
S10/8-2 Ad		7.75	125–180	0.99 ± 0.07	0.45 ± 0.03	0.18 ± 0.02	1.63 ± 0.05	24(24)	CAM	23 ± 1	14 ± 1
S10/8-3 Ad		7.25	125–180	1.02 ± 0.07	0.46 ± 0.03	0.18 ± 0.02	1.66 ± 0.05	21(24)	FMM	17 ± 1	10 ± 1
S10/9-1 Ad	5d	0.66	125–180	0.68 ± 0.05	0.41 ± 0.03	0.20 ± 0.02	1.30 ± 0.03	24(24)	CAM	14 ± 1	11 ± 1
S10/9-2 Ad		0.60	125–180	0.71 ± 0.05	0.42 ± 0.03	0.20 ± 0.02	1.34 ± 0.04	24(24)	FMM	16 ± 2	12 ± 2
S10/10-1 Ad	5f	0.85	125–180	0.87 ± 0.06	0.41 ± 0.03	0.19 ± 0.02	1.48 ± 0.05	24(24)	CAM	0.1 ± 0.1	0.1 ± 0.1
S10/10-2 Ad		0.95	125–180	0.92 ± 0.06	0.43 ± 0.03	0.19 ± 0.02	1.54 ± 0.05	24(24)	CAM	0.1 ± 0.1	0.1 ± 0.1
*S11/WN1 Ab		0.00	180–212	0.65 ± 0.04	0.30 ± 0.02	0.20 ± 0.02	1.25 ± 0.06	24(24)	CAM	0.00 ± 0.02	0.00 ± 0.02
S11/A2-1 Ab	5c	0.65	180–212	0.55 ± 0.02	0.31 ± 0.02	0.20 ± 0.02	1.06 ± 0.03	22(24)	CAM	7.7 ± 0.5	7.3 ± 0.5
S11/A2-2 Ab		0.75	180–212	0.55 ± 0.02	0.31 ± 0.02	0.19 ± 0.02	1.05 ± 0.03	24(24)	CAM	9.6 ± 0.4	9.2 ± 0.5
S11/A2-3 Ab		1.00	180–212	0.59 ± 0.03	0.30 ± 0.01	0.19 ± 0.02	1.07 ± 0.04	22(24)	CAM	11 ± 1	10 ± 1
*S11/1-1 Ab	3f	1.20	180–212	0.99 ± 0.04	0.45 ± 0.02	0.18 ± 0.02	1.62 ± 0.05	22(24)	CAM	112 ± 6	69 ± 4
*S11/1-2 Ab		1.50	180–212	0.90 ± 0.04	0.41 ± 0.02	0.17 ± 0.02	1.48 ± 0.04	23(24)	CAM	130 ± 6	

(*continued on next page*)

Table 1 (*continued*)

Sample	Section/Fig. no.	Depth (m)	Grain size (μm)	Beta[1]	Gamma[1]	Cosmic	Total	Num. Aliquots	Age Model	De (Gy)	Age (ka)
*S11/1-3 Ab		2.35	180–212	0.83 ± 0.04	0.38 ± 0.02	0.16 ± 0.04	1.36 ± 0.06	21(24)	CAM	140 ± 10	88 ± 5
S11/2-3 Ab	3a	6.70	150–212	0.32 ± 0.02	0.21 ± 0.01	0.10 ± 0.05	0.63 ± 0.05	22(24)	CAM	170 ± 8	103 ± 9
S11/2-4 Ab		2.90	150–250	0.30 ± 0.02	0.29 ± 0.01	0.15 ± 0.08	0.74 ± 0.08	22(24)	CAM	140 ± 6	270 ± 30
S11/2-5 Ab		0.75	150–212	0.95 ± 0.04	0.56 ± 0.02	0.19 ± 0.07	1.70 ± 0.08	19(24)	CAM	89 ± 11	190 ± 20
*S11/3-1 Ab	3c	0.80	180–212	0.80 ± 0.03	0.38 ± 0.02	0.19 ± 0.04	1.36 ± 0.05	22(24)	CAM	140 ± 7	52 ± 7
											104 ± 6

Notes: 1. A water content of 5 ± 2% was assumed for all samples except the modern sample from the White Nile (WN1) for which a water content of 10 ± 5% was assumed, and samples SU10/3-1, SU10/3-2, SU10/6-2, SU10/6-3 and SU10/6-4 which had measured water contents of over 20%. For these samples the measured water content was used in the dose rate calculations. The beta and gamma dose rates given here are after attenuation for water content and grain size. Ab indicates samples analysed at Aberystwyth; Ad those analysed at Adelaide.

Table 2
Radiocarbon ages of samples from the White Nile, Blue Nile and Dinder valleys, central Sudan. Calibrated using software package of Fairbanks et al. (2005).

Field sample no	Section/Fig. no.	Laboratory no	Material	Uncalibrated age (yr BP)	Calibrated age (cal yr BP)_
S82/14	3b	OZE-587	Oyster shell	38, 820 ± 330	43,150 ± 400
S10/6-5	3g	Wk-28054	Mussel shell	33,736 ± 140	39, 113 ± 203
S10/6-9		Wk-28058	Mussel shell	104.8 ± 0.5	Modern
S10/6-7		Wk-28056	Mussel shell	36,066 ± 991	41,303 ± 906
S10/6-8		Wk-28057	Mussel shell	47,814 ± 412	Beyond range
S10/8-4	3h	Wk-28051	Mussel shell	11,094 ± 38	12,952 ± 42
S10/8-5		Wk-28052	Mussel shell	11,572 ± 40	13,438 ± 42
S10/8-6		Wk-28053	Mussel shell	11,082 ± 96	12,943 ± 85
S11/2-2	3a	Wk-30975	Oyster shell	35,656 ± 490	40,949 ± 477
S11/2-1		Wk-30976	Oyster shell	38,486 ± 600	43,411 ± 545
S11/4-1		Wk-30973	Charcoal	2849 ± 30	2951 ± 43
S11/4-3		Wk-30974	Mussel shell	1165 ± 25	1069 ± 35
S11/4-2		Wk-30889	Ostrich eggshell	1770 ± 25	1689 ± 35

consisted of planar and cross-bedded loose dry sand throughout (Fig. 5: section 5f). At both 85 cm and 95 cm depth the OSL age was not significantly different from zero (Table 1; Fig. 5: site 5f), indicating that this dune had been very recently reactivated.

In 2010 sand samples were collected from a 1.67 m deep pit dug in a dune located east of the Sabaloka cataract on the main Nile at 16°24.239′ N and 32°41.425′E (Fig. 1b; Fig. 5: site 5g). This dune formed part of a complex of stable older red dunes overlying rolled Nubian Sandstone gravels that represented either a higher Nile flood level or local wadi gravels graded to a higher Nile. The OSL ages were 5.6 ± 0.3 kyr at 33 cm depth, 6.2 ± 0.4 kyr at 63 cm depth and 9.4 ± 0.6 kyr at 107 cm depth (Table 1). The ages are all in consistent stratigraphic order and denote vertical accretion of the dune during the early and middle Holocene. These three ages coincide with times of rapid climate change, polar cooling and tropical aridity identified by Mayewski et al. (2004).

Table 3
^{36}Cl exposure ages for moraines in the Semien Highlands, Ethiopia.

Sample ID	Age (kyr)
Mount Bwahit	
BUW 01	32.7 ± 1.4
BUW 08	15.3 ± 0.7
BUW 10	68.5 ± 3.5
Mount Mesarerya	
MSA 01	27.4 ± 1.0
MSA 04	36.4 ± 1.6
MSA 07	18.1 ± 0.9
MSA 10	46.2 ± 2.1

6. Holocene environments in the main Nile valley, northern Sudan

The most recent period of sapropel deposition in the Eastern Mediterranean ended around 6.0 kyr ago (Thomson et al., 1999) at the end of the so-called African Humid Period. If we consider the NDR records in relation to the formation of Sapropel 1 in the Eastern Mediterranean, the earliest Holocene ages are of particular interest. Those sites where we have well dated evidence of fluvial sedimentation by the main Nile before 5.5 kyr are shown on Fig. 6b. We have ten OSL ages >5.5 kyr and 6 of these are older than 6 kyr. Macklin et al. (2013) provide full details of all OSL ages and dating procedures used in the NDR study. Significantly, these ages show that all of the channel belts in the NDR as well as the modern Nile conveyed permanent flows at this time. The NDR was a multiple channel system in the early Holocene with a series of large islands. The presence of Neolithic settlements across the study area on all of the channels belts at this time (Fig. 6a) provides independent evidence in support of a much greater area of the valley floor occupied by flowing channels before 5.5 kyr than is seen today. Floodwater farming was probably widespread at this time making use of the enhanced Nile flows.

The dated records from pits 38 and 40 in the far northeastern sector of this reach (Fig. 6b) show that the early Holocene Nile was flowing close to the bedrock plateau at this time. Plate 6 shows the sedimentary record exposed in pit 40 with thick deposits of grey Nile silts. Interestingly, the OSL age of 8.4 ± 0.3 kyr was obtained from a distinctive bed of windblown orange sand that may represent a brief interval of dry climate and reduced flows during the deposition of Sapropel 1. This may correlate with the 8.2 kyr event

Table 4
Late Quaternary fluctuations in the Blue Nile hydrological cycle.

(a) The Blue Nile at 21-18 kyr BP
- Glacial cooling and aridity in Ethiopia.
- Weaker monsoon and less summer rain.
- Small cirque glaciers above 4200 m in the Semien Mountains.
- Winters 4–8 °C cooler.
- Slopes unstable down to 3000 m, with periglacial solifluction mobilising abundant coarse debris.
- Treeline 1000 m lower in Blue Nile headwaters.
- Savanna/desert ecotone higher.
- High seasonal runoff, leading to high peak flows but overall annual discharge much reduced.
- Blue Nile has a braided stream channel with sand and gravel point-bars.
- Distributary channels radiate out from the lower Blue Nile across the Gezira alluvial fan.
- Dry season deflation of channel sands and formation of source-bordering dunes at distal end of distributary channels.
- Coarse alluvial sands and gravels deposited in northern Sudan and southern Egypt.
- Flow to and in the Main Nile highly seasonal, with much reduced winter flow.
- In very dry years the Main Nile probably dries out into a series of pools.

(a) The Blue Nile at 15–14 kyr BP
- Postglacial warming and return of the strong summer monsoon.
- Longer wet season and increased summer rainfall.
- Winters 4–8 °C warmer and cirque glaciers melt and disappear.
- Slopes above and below 3000 m in headwaters region now vegetated and stable.
- Treeline 1000 m higher in the headwaters.
- Lowland savanna expands across former semi-desert.
- Tuffs and basalts in the Ethiopian Highlands weather to form clay soils.
- Seasonal erosion of uplands clays provides Blue Nile with an abundant suspension load of silt and clay.
- Higher annual discharge and enhanced base flow, with attenuated flood peaks, but river still highly seasonal.
- Perennial flow re-established and prolonged widespread flooding in central Sudan by sinuous and straight distributary channels.
- High seasonal discharge into the Main Nile together with seasonally high suspension load.

(Rohling and Pälike, 2005). Several exposures in the eastern part of the NDR also preserve evidence of flooding from local wadis draining the bedrock plateau before 5.5 kyr. It is likely that these deposits were produced under a more humid climatic regime when the ITCZ encroached into this part of the Africa.

Several lines of evidence therefore point to the presence of higher Nile flows in the NDR in the period before 5.5 kyr. The Qaab Depression would have received water from the main Nile when all of the major valley floor channel belts (Dongola, Hawawiya, Alfreda, and Seleim) were active. Together with the OSL-dated alluvial record in the Northern Dongola Reach, the Qaab lake record shows that this reach of the Nile was a multiple channel system that conveyed much higher discharges than present in the earliest Holocene and throughout the period of formation of Sapropel 1.

A major change took place with the onset of the Kerma Period at 2400 BC when all archaeological sites in the NDR were located on the margins of the channel belts as the climate became drier and Nile flows decreased. Some of the smaller channels on the valley floor ceased to flow at this time. The detailed record of river channel dynamics and human–environment interactions through the Neolithic, Kerma and later periods is set out in Macklin et al. (2013). It is important to point out that meta-analysis of the OSL and radiocarbon records from multiple sites across the Nile basin is beginning to show a higher resolution record of Holocene hydrological change in the region with evidence for millennial- and centennial-scale change in river flows within the broader pattern of change presented here.

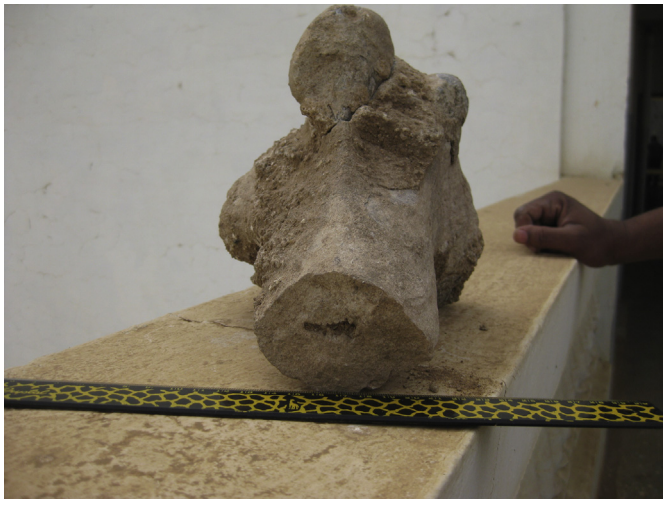

Plate 2. Fossil rhinoceros bones retrieved from late Pleistocene (100 kyr) alluvial sands and fine gravels adjacent to the present Blue Nile, 2 km south of Branko village, central Sudan. The scale is 30 cm long.

Plate 3. Aerial photograph showing meandering Blue Nile palaeochannels 15 km east of the lower White Nile, central Sudan. The channels were active between 100 and 50 kyr ago, and are flanked and partly obscured by Holocene clays and sporadic sand dunes. Fig. 3a, site 3d shows the location. The top of the photograph is north. The photo covers 5.75 km × 5.75km. The palaeochannels are ca. 200-250 m wide.

Plate 4. Satellite image showing terminal Pleistocene and early Holocene Blue Nile palaeochannels and sand north of Singa, central Sudan. Fig. 1b, site 3h shows the location. The top of the image is north. The image covers 85 km × 45 km.

7. Discussion

7.1. Climate, vegetation and sediment output from the Ethiopian Highlands

A number of boreholes were drilled to depths of several hundred metres across the Gezira during a programme of groundwater prospecting in the 1970s. One of us (MAJW) examined the core samples and found a series of fining-upwards cycles evident in the stratigraphic record. Each cycle consisted of a basal unit of fluvial sands and gravels and an upper unit of grey-brown clay. El Boushi and Abdel Salam (1982) mapped a series of sub-surface sandy palaeochannels that radiated across the Gezira from southeast to northwest. As noted earlier, the Gezira is a vast low-angle alluvial fan laid down by the Blue Nile and its Ethiopian tributaries during the Quaternary and abutting along its western margin onto the Quaternary flood plains of the White Nile.

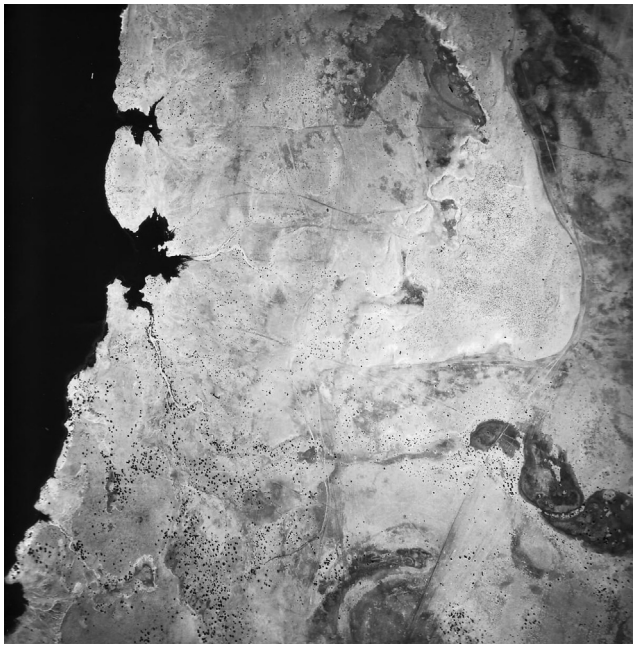

Plate 5. Aerial photograph showing now vegetated and stable linear sand dune located 2.5 km east of the lower White Nile, central Sudan. This dune was intermittently active during the last 50 kyr. Holocene flood plain clays are banked against the dune. Fig. 3a, site 5a shows the location. The top of the photograph is north. The photo covers 5.75 km × 5.75 km. The southern dune base is 1.75 km wide from east to west.

Plate 6. Holocene sedimentary record exposed in Pit 40. The arrow points to the sand unit that yielded the OSL age. The OSL sample was collected at a depth of 3.35 m below the modern land surface.

Thirty five years ago, when far fewer radiometric ages were available for this region, Adamson et al. (1980) and Williams and Adamson (1980) proposed a simple depositional model linked to climate and changes in plant cover in the Blue Nile and Atbara headwaters (Fig. 7) to account for these changes. During cold, dry glacial intervals the headwaters of major Ethiopian rivers would be sparsely vegetated, hill slope erosion would be accelerated and rivers would become highly seasonal, low-sinuosity, bed-load streams which transported large volumes of poorly sorted sands and gravels. Conversely, with a return to warm, wet conditions and re-establishment of a dense plant cover in the headwaters, we should see a change to high-sinuosity, suspended load streams that carried and deposited silts and clays. A fining-upwards alluvial sequence from coarse basal gravels through sands to horizontally bedded silts and clays is thus a predictable outcome of a change from bed-load to suspended-load regime, related to a change from glacial aridity to interglacial and postglacial climatic amelioration.

The precise timing of the last glaciation in the Ethiopian Highlands is still being investigated. Because of an absence of organic material in association with the moraines or outwash, it has not been possible to determine closely limiting or bracketing radiocarbon dates. Osmaston et al. (2005) considered that up to 180 km^2 of the Bale Mountains of Ethiopia (Fig. 1a) could have been glaciated during the last glacial, with a central ice cap of at least 30 km^2. Moraines and periglacial deposits in the Semien Mountains near the sources of the Tekezze and Blue Nile/Abbai rivers (Fig. 7) are presently being exposure dated using the cosmogenic nuclide ^{36}Cl (Table 3). The first seven ages obtained so far show that moraines associated with two sets of cirque glaciers have ^{36}Cl exposure ages of 68.3 ± 3.5, 37.7 ± 1.4 and 15.3 ± 0.7 kyr for the cirque on the north face of Mt Bwahit (13°15.6′N and 38°11.5′E; elevation 4430 m) and 46.2 ± 2.1, 36.4 ± 1.6, 27.4 ± 1.0 and 18.1 ± 0.9 kyr for the cirque on the northwest face of Mt Mesarerya (13°12.8′N and 38°12.8′E; elevation 4353 m) (Barrows et al., unpublished data). Sample preparation methods and age calculations follow Barrows et al. (2013). Some of the older ages may denote inheritance of ^{36}Cl from older erosional surfaces due to shallow glacial erosion in these small cirques rather than a prolonged period of glaciation. Nevertheless, ice was present on Mt Mesarerya 18.1 kyr ago and on Mt Bwahit 15.3 kyr ago. The mapped lower limits of periglacial solifluction deposits in the Semien Mountains point to colder late Pleistocene, possibly Last Glacial Maximum (LGM) conditions (4–8 °C cooler) with a lowering of the upper tree line by ~1000 m during that time (Williams et al., 1978; Hurni, 1982).

As noted earlier, the presence or absence of glaciers in the headwaters region of the Tekazze/Atbara has important consequences downstream. Although the headwaters of the Abbai/Blue Nile do not emanate directly from the Semien Mountains, high mountains within the Blue Nile catchment area, such as Mt Guna (with an elevation of 4231 m) which lies only 160 km to the south of the Semien Mts would most likely have experienced a similar history.

7.2. Nile discharge and sapropel formation in the eastern Mediterranean

There have been many very useful attempts to use variations in the physical and chemical properties of marine sediments obtained from deep-sea cores in the eastern Mediterranean to reconstruct past variations in Nile discharge and sediment flux (Ducassou et al., 2008, 2009; Rohling et al., 2009; Revel et al., 2010; Zhao et al., 2011, 2012; Blanchet et al., 2013; Hennekam et al., 2014). These studies have almost invariably concluded that during phases of inferred very high Nile flow clastic muds rich in continental organic matter and highly organic sapropels accumulated on the floor of the eastern Mediterranean (Rossignol-Strick et al., 1982; Rossignol-Strick, 1985, 1999; Lourens et al., 1996; Larrasoaña et al., 2003; Ducassou et al., 2008, 2009).

Zhao et al. (2012) used fluctuations in the ratio of iron to aluminium (Fe/Al) in marine core MD90-964 on the distal Nile fan in the Levantine Basin of the eastern Mediterranean as a measure of changes in inputs of Fe-bearing heavy minerals transported by the Nile from its Ethiopian headwaters and, indirectly, as a proxy for changes in precipitation in that region. They found that times of peak values in the Fe/Al ratio coincided with times of sapropel formation as well as some periods in between. Spectral analysis of the Fe/Al fluctuations showed a 23-kyr precessional cycle, from which they concluded that precipitation changes in the Ethiopian Blue Nile and Atbara River headwaters reflected changes in the intensity of the African monsoon. They cited earlier studies based on Sr and Nd isotopic ratios and clay mineral composition of sapropels, which suggested reduced terrigenous input from the Nile during sapropel formation, whereas studies of heavy minerals indicated higher Nile discharge during monsoon maxima (Foucault and Stanley, 1989; Revel et al., 2010). This apparent contradiction was not explained.

In an earlier study, Zhao et al. (2011) obtained a record of oxygen isotope variations in marine core MD90-964 extending back to 1.75 Ma. They identified 21 sapropel layers (characterised by organic carbon contents of at least 1%) and a further 21 dark layers enriched in Ba but in which the carbon had been oxidised and removed, which they termed “ghost sapropels” and “hidden sapropels”. They used fluctuations in Ti and V as a proxy for fluctuations in Nile suspended sediment flux from the Ethiopian headwaters, which revealed a strong precessional signal as well as a more enigmatic 78-kyr signal. They noted that during times when the African monsoon was more intense precipitation would have been greater in the Ethiopian Highlands, resulting in higher runoff from the Atbara and Blue Nile. However, they also noted that higher rainfall would lead to a denser vegetation cover and hence less erosion. They concluded that fluctuations in Nile sediment discharge ‘are more the result of river transport capability than of erosion potential in source areas’ (Zhao et al, 2011, p. 239).

These studies indicate that the factors governing Nile discharge and Nile sediment load are complex. Some insights into the processes governing sediment yield come from field monitoring in the seasonally wet tropics of northern Australia. At the hill slope scale, runoff plot measurements from this region show rates of soil detachment from raindrop impact up to 40 times greater for the same unit momentum of raindrop impact at the start of the wet season when the soil surface is bare than four months later when the plant cover is at a maximum (Williams, 1969, 1978). This sediment remains in temporary storage on the hill slopes until the streams and rivers are in flood, when it is carried out to sea. Once the initial pulse of sediment has been moved, discharge remains high but sediment load diminishes (Williams, 1976). These observations can be applied to the Nile.

Blue Nile discharge is forty times greater in August, at the height of the wet season, than in May at the end of the dry season (Williams et al., 1982, Table 7.1). Suspended sediment concentration at Khartoum is forty times greater in August than in May (El Badri, 1972; Williams et al., 1982), so that during peak flow the Blue Nile transports nearly two thousand times more sediment in suspension than during the month of minimum flow. As water discharge slowly diminishes we might expect a more rapid reduction in sediment flux than in water flow, because sediment transport is a power function of stream velocity, which is in turn proportional to discharge.

Recent work in the Snowy Mountains of southeast Australia provides additional insights into reasons for possible high seasonal

rates of runoff from the Ethiopian headwaters of the Blue Nile and Atbara during times of much lower glacial temperatures. Reinfelds et al. (2014) found that in the Snowy Mountains detailed measurements of precipitation, temperature, evaporation and runoff revealed that runoff decreased by 17% for every 1° increase in annual temperature. On the basis of this observation, and assuming the converse to apply, they suggested that lower LGM temperatures in that region could have more than doubled runoff, thereby providing an explanation for the very large late Pleistocene palaeochannels visible on the surface of the Australian Riverine Plain. Lower glacial temperatures in the Semien Mountains of Ethiopia may have been associated with very high rates of seasonal runoff from the Tekezze/Atbara and Blue Nile, enabling these rivers to ferry a substantial load of coarse sand and gravel into northern Sudan and southern Egypt during glacial intervals in the late Pleistocene. Such coarse alluvial deposits are present in that region but their origin has never been adequately explained.

There are two further sources of complexity when seeking to interpret events upstream relying solely on the distal marine sediment record. One concerns the relative sediment contributions from the Blue and White Nile (Foucault and Stanley, 1989; Blanchet et al., 2013). According to Blanchet et al. (2013), marine core P362/2-33 collected from the Nile deep-sea fan shows that the relative intensity of Blue Nile discharge was greater during the early and late Holocene when spring insolation was high in the Blue Nile headwaters but was reduced between 8 and 4 kyr ago, when autumn insolation was high and the White Nile came to the fore. The core also revealed evidence of an arid event at 8.5–7.3 kyr and again at 4.5–3.7 kyr.

The second source of complexity concerns the nature of material transported by the White Nile. During times of extreme aridity in East Africa, flow from the Ugandan lakes would be eliminated, White Nile flow would virtually cease, and the Sudd swamps in South Sudan would dry up. With the return of the summer monsoon, the Ugandan lakes would overflow and flow would resume in the White Nile. Until the Sudd had time to become re-established, White Nile discharge would be very much greater (because there would be no losses to seepage and evaporation in the Sudd), the flow regime far more seasonal, and the load transported would be much greater and far coarser, as shown in the large sandy cross-beds exposed in a sand quarry near Ed Dueim west of the present river (Williams et al., 2010). Once the Sudd became fully established the White Nile flow regime would again change and become less seasonal. (The ratio of high to low flow in the White Nile today is 2.5: 1; that of the Blue Nile 40:1; that of the Main Nile 16:1). At present about half the total annual discharge of the White Nile entering the Sudd, amounting to 20 km^3, is lost to evapotranspiration and seepage, and much of the sediment load is trapped in the Sudd. Only a few million tonnes of fine suspended sediment travel downstream.

Tables 4 and 5 are an attempt to summarise the changes in discharge and sediment yield in the Blue and White Nile catchments during the last 21 kyr. The LGM (21 ± 2 kyr) in Ethiopia was in general very much drier than today with lakes in the Afar and Ethiopian Rifts shallow and saline or dry (Gasse, 2000a). However, temperatures were also much lower, so that snow persisted on the higher summits of the Semien and Bale Mountains, and small cirque glaciers (such as those on Mt Bwahit and Mt Mesarerya discussed in section 7.2) were present in the vicinity of the Tekazze/Atbara headwaters and, most probably, the upper basin of the Abbai/Blue Nile. Both rivers were even more seasonal than today with high flood peaks during the spring and early summer, enabling them to transport a bed load of coarse sand and gravel across the Gezira and into northern Sudan and southern Egypt, where it accumulated to form gravel terraces. With the return of a strong summer monsoon from 15 kyr onwards (Gasse, 2000b), there was a change in the type of sediment carried by the Blue Nile. No longer a bed load stream ferrying sand and gravel, the Blue Nile and its major tributaries, the Rahad, Dinder and Sobat, now began to transport a sizeable suspension load of silt and clay. Some of this clay was deposited across the surface of the Gezira, some along the flood plain of the Main Nile, but most of it reached the Mediterranean and accumulated on the Nile cone and delta.

7.3. East Mediterranean sapropel chronology

Before discussing the links between sapropel formation and intervals of very high flooding in the lower Atbara, Blue and White Nile valleys, we need to consider the scope and limitations of sapropel chronology in the eastern Mediterranean. Lourens et al. (1996) have provided a comprehensive review of every sapropel identified in the Mediterranean until that time, with ages inferred from oxygen isotope stratigraphy in deep-sea cores calibrated against the astronomical time scale. The ages they cite are midpoint ages and do not show the age range of each sapropel. Many workers have noted that individual sapropels can be missing from adjacent marine sediment cores or can vary in thickness. Differential oxidation of the organic carbon within a sapropel is the main reason for this, and helps to explain the widely different age estimates for the youngest and best preserved of all the sapropels: sapropel S1. Ages proposed for S1 range from 12 to 6 kyr (Cramp and O'Sullivan, 1999), 13.7–12.4 near the base and 9.9–8.9 near the top (Ducassou et al., 2009), 9.5–6.6 kyr (Revel et al., 2010), and 10.1–6.5 kyr with a gap at 8.2–7.9 kyr (Hennekan et al., 2014). Reference to figures 4 and 5 in Ducassou et al. (2009) suggests ages of 55 ± 1 kyr for S2 (MIS 3), 78–82 kyr for S3 (MIS 5a), 96–100 kyr for S4 (MIS 5c), 118–125 kyr for S5 (MIS 5e), 170–180 kyr for S6 (MIS 6) and 194–200 kyr for S7 (MIS 7). All of the Marine Isotope Stages specified are warm intervals except for MIS 6, which is a cold interval. Cramp and O'Sullivan (1999) noted that sapropel S8 also coincides with a cold climatic interval in the Mediterranean, and commented that sapropel S2 is often missing or not visible. Given these caveats, the ages proposed for each sapropel should be considered best present estimates only. The ages we cite in section 7.4 are those of Lourens et al. (1996) unless specified otherwise.

7.4. Blue and White Nile flood phases and associated sapropel formation in the eastern Mediterranean

Fig. 8 shows phases of high Nile floods, as determined in this study, in relation to dated intervals of sapropel formation in the East Mediterranean during the last 125 kyr. Sapropel 5 (124 kyr) was synchronous with major flooding and the creation of an enormous seasonal lake in the White Nile valley (Barrows et al., 2014) and with a prolonged wet phase at ~125 kyr at Kharga Oasis in the Western Desert of Egypt (Kieniewicz and Smith, 2007). The final stages of the White Nile mega-lake and its regression dated to 109 kyr, after which it never filled to such a high level. Recently dated high flood deposits on the main Nile are coeval with sapropel unit S3 (81 kyr) (Williams et al., 2010). Each sapropel unit probably encompasses an episode several thousand years in duration of above average floods in the Nile.

Until now there have been no well-dated terrestrial fluvial sediments from the Nile synchronous with sapropel unit S2 (55 kyr) and S4 (102 kyr). Our 50–60 kyr ages for the Nile oyster-bearing clays at Masoudia, for the shells and silty clays in the banks of the Dinder river near the Ethiopian border, for the sandy clay near the base of the linear dune, and for the uppermost fluvial sands in the Artimeili palaeochannel are all consistent with a major wet phase at about this time. For the first time we now also have

Table 5
Late Quaternary fluctuations in the White Nile hydrological cycle.

(a) The White Nile at 21–18 kyr BP
- Glacial aridity.
- Ugandan lakes low or dry.
- No overflow into White Nile.
- Sudd swamps and Machar Marshes in South Sudan dry out.
- White Nile flow reduced to a trickle.
- Dunes block the channel of the lower White Nile south of Khartoum.

(b) The White Nile at 18–15 kyr BP
- Postglacial warming and increase in summer precipitation.
- Ugandan lakes refill and overflow into South Sudan.
- Sudd swamps not yet re-established.
- Significant increase in White Nile discharge.
- White Nile annual flow regime more seasonal
- White Nile transports a significant bed load of medium to fine sand as well as a large suspended load of silt and clay.
- Widespread flooding in the lower White Nile valley.
- White Nile becomes a major contributor of water and sediment to the Main Nile.

(c) The White Nile at 15–11 kyr BP
- Summer monsoon remains strong.
- Sudd swamps and Machar Marshes in South Sudan re-established.
- Roughly half the water flowing into the Sudd lost to seepage and evapotranspiration.
- Sudd operates as a gigantic physical and chemical filter.
- White Nile discharge roughly halved and sediment load reduced to minor amounts of suspended clay.
- Flow regime buffered by Ugandan lakes and swamps and far less seasonal.
- White Nile becomes an important contributor to Main Nile during the drier months, when discharge from the Atbara and Blue Nile is severely curtailed.

ages of major Blue Nile flooding at ~100 kyr at the Branko fossil sites, and in the Artimeili palaeochannel sands, coeval with sapropel S4 (102 kyr).

The oldest Blue Nile palaeochannels exposed on the surface of the Gezira alluvial fan date were synchronous with or slightly younger than sapropel S5 and remained active during the formation of S4, and both before and after the formation of S3, after that of S4, and during that of S1 (Fig. 8). Deposition of the Blue Nile flood plain clays was coeval with the formation of S3, S2 and S1, and continued between the formation of S3 and S2. The Dinder flood plain silts were accumulating during and after the formation of sapropel S2. Floods along the Main Nile precede the formation of sapropel S5 and S1, but also coincide with S3 and S1. In the middle Atbara valley, floods were synchronous with S5 (last interglacial) and, possibly, with S4 (Abbate et al., 2010). Source-bordering dunes in the lower White Nile valley were active during the formation of S1, S2 and during or after the formation of S5.

Older flood deposits exposed in trenches dug east of the present White Nile near Esh Shawal village 265 km south of Khartoum (Williams et al., 2003) show episodes of middle to late Pleistocene high flow (Fig. 2b) which may or may not, coincide with sapropel units S8 (217 kyr), S7 (195 kyr) and S6 (172 kyr) (Lourens et al., 1996), but the error terms are too large to allow any definite correlations. These were all times when the White Nile was depositing fine sand and clayey sand across its flood plain.

The most recent sapropel S1 in the eastern Mediterranean is a composite unit, with ages of 13.7–12.4 kyr near the base and 9.9–8.9 kyr near the top (Williams et al., 2010). The gap in the S1 record may coincide with the arid phase seen in other parts of Africa coeval with the Younger Dryas (~12.5–11.5 kyr). Higgs et al. (1994) considered that formation of sapropel S1 may have ended as recently as 5 kyr ago, which is also when the Nile deep-sea turbidite system became inactive as a result of reduced sediment discharge from that river (Ducassou et al., 2009). The interval from ~13.7 to 8.9 kyr and locally up to 5 kyr, also coincides with a time when freshwater lakes were widespread in hollows between the White Nile dunes (Adamson et al., 1974; Williams and Nottage, 2006), as well as west of the Nile and in the eastern Sahara (Williams et al., 1974; Ayliffe et al., 1996; Abell and Hoelzmann, 2000; Hoelzmann et al., 2004; Williams et al., 2010; Williams and Jacobsen, 2011) and when the White Nile attained flood levels up to 3 m above its modern unregulated flood level. In the desert Nile of northern Sudan well-dated archaeological and geomorphological data demonstrate the presence of more numerous and wider river channels (and therefore much larger Nile flows) during this period (Woodward et al., 2001; Macklin et al., 2013).

It is interesting to note that McDougall et al. (2008) also correlated rapid deposition of three well-dated members of the Kibish Formation in the lower Omo valley with sapropel units in the Mediterranean. Member 1 (196 kyr) was coeval with sapropel S7 (195 kyr), Member III (104 kyr) with sapropel S4 (102 kyr) and Member IV (9.5–3.3 kyr) with sapropel S1. These were all times of stronger summer monsoon, with Lake Turkana 20–40 m deeper and overflowing into the White Nile via the Pibor and Sobat rivers. In addition, the headwaters of the Omo and Blue Nile share a common divide, consistent with very high flow in the Blue Nile at those times, as discussed earlier.

In the middle Atbara valley, Abbate et al. (2010) have identified two major Pleistocene fluvial formations rich in fossils and prehistoric stone tools. The younger of the two alluvial formations contains abundant vertebrate remains and late Acheulian to Middle Stone Age artefacts. It comprises three sub-formations. From the base up these are sands from meandering rivers; braided river deposits evolving into sinuous river sands; and braided river pebbly sands and sheet flow deposits. Two U/Th ages of 126.1 ± 1.0 kyr and 92.2 ± 0.7 kyr obtained from mollusc patch reefs with stromatolite coatings at the base of the two younger sub-formations indicate that the river became active during MIS 5e and MIS 5c, coeval with sapropel units S5 and S4, respectively. The oldest sub-formation was attributed to MIS 7, coeval with sapropel S7, but in the absence of any radiometric ages this inference remains conjectural.

Where independently dated comparisons exist between sapropel formation and Nile floods, they point to synchronism between sapropel accumulation and times of higher Nile flow, indicative of a stronger summer monsoon at these times. Although the sapropel record in the eastern Mediterranean is incomplete, with some evidence of complete removal of sapropels by post-depositional oxidation (Higgs et al., 1994), it is a longer and more complete record than that presently available on land. It follows that if our conclusions are correct, and sapropel units do indeed coincide with

episodes of very high Nile flow, then the older sapropel record may point to as yet undated phases of very high Nile discharge earlier in the Pleistocene.

The Blue Nile has cut down at least 10 m since ~15 kyr and at least 4 m since 9 kyr, with concomitant incision by the White Nile amounting to 4 m since ~15 kyr and at least 2 m since 9 kyr (Arkell, 1949, 1953; Williams and Adamson, 1980; Williams et al., 2000). Such incision would help to drain previously swampy flood plains, freeing them for Neolithic and later cultivation. A number of episodes of high Nile floods occurred during this time and are reflected in the presence of cross-bedded sands and shell-bearing clays above the maximum unregulated flood levels. Thanks to a very gentle flood gradient (1:100,000) the post-LGM flood deposits in the lower White Nile valley are well preserved. Calibrated ^{14}C ages obtained on freshwater gastropod and amphibious *Pila* shells and fish bones show high White Nile flood levels around 14.7–13.1, 9.7–9.0, 7.9–7.6, 6.3 and 3.2–2.8 kyr. The less complete Blue Nile record shows very high flood levels towards 13.9–13.2, 8.6, 7.7 and 6.3 kyr (Williams, 2009).

Mayewski et al. (2004) synthesised the results from some fifty globally distributed Holocene paleoclimate records spanning the time interval from 11.5 kyr to present. They identified six significant periods of rapid climate change during 9–8, 6–5, 4.2–3.8, 3.5–2.5, 1.2–1.0 and 0.6–0.15 kyr, the first five of which coincided with polar cooling and tropical aridity. The intervals in between were wetter in the tropics and, allowing for dating errors, tally reasonably well with the intervals of high Blue and White Nile floods identified here. A more detailed record of times of high and low precipitation in the White Nile headwaters region comes from Lake Challa on the eastern flank of Mt Kilimanjaro (Verschuren et al., 2009). The lake was high between 14 and 13 kyr and again very high between 10.5 and 8.5 kyr. Levels were low during 12.8–12.4, 8.0–6.7, 5.9–4.7, 3.6–3.0 and 0.7–0.6 kyr. The intervals between or after these times of low lake level were relatively wet and are in reasonable accord with the White Nile Holocene chronology. At the site of Erkowit in the Red Sea Hills (Mawson and Williams, 1984) there is evidence of permanent stream flow towards 1.8–1.6 kyr, coinciding with high White Nile flows but not so far evident in the much more incomplete Blue Nile sedimentary record.

8. Conclusion

The results of our work in 2010 and 2011 show that the surface palaeochannels that cross the Gezira were active from at least 103 kyr ago to about 5 kyr ago, and that the dunes between Jebel Aulia and Wad ez Zaki are of similar age. The earliest surface deposits of Gezira clay were laid down 50 kyr ago, when there was a major change in the flow regime of the Blue Nile and Dinder associated with a stronger summer monsoon. We now have luminescence ages for the near-surface Blue Nile gravels near Masoudia south of Khartoum indicating that the Blue Nile was actively transporting gravel in this area over 250 kyr ago. Finally, the rhinoceros fossils near Branko village some 150 km upstream of Khartoum on the east bank of the Blue Nile are 104 ± 6 kyr old, at which time there was also a major change in Blue Nile flow regime and more intense summer rains. The Gezira is thus a polygenic low-angle alluvial fan, some parts of which were laid down during the Holocene, and others at intervals between at least 250 kyr and 15 kyr ago.

Two major achievements of the 2010 and 2011 field seasons in the lower Blue and White Nile valleys have been to extend the documented Quaternary flood history of the Blue Nile back from 15 kyr to at least 270 kyr and to obtain a chronology for the palaeochannels visible on the surface of the Gezira fan extending back to at least 103 kr, coincident with sapropel S4 (102 ka) in the eastern Mediterranean. Other achievements include establishing a chronology for the vegetated linear dunes immediately east of the White Nile extending back to at least 115 kyr, and to demonstrate a major change in depositional regime in the Blue Nile and Dinder rivers at ~55 kyr synchronous with sapropel S2 (55 kyr). Our results have confirmed the close relationship that exists between times of sapropel accumulation in the eastern Mediterranean and independently dated evidence of major fluvial activity in both the Blue and the White Nile valleys during the last 125 kyr. They have also shown that times of widespread clay deposition by the Blue Nile were slightly out of phase with times when Blue Nile distributary channels were carrying a bed load of sand and gravel across the Gezira alluvial fan. The clay flood plain deposits coincide with summer monsoon peaks while the channel sands indicate somewhat drier and more seasonal conditions in the headwaters, with a reduced annual discharge but high seasonal peak flows.

Acknowledgements

We thank the Australian Research Council for financial support (ARC Grant DP0878058 to MAJW) and Professor Eduardo Garzanti and an anonymous reviewer for fertile comments. Particular thanks go to Dr Abdelrazig Ahmed and Dr Yusif Elsamani (respectively, past and present Directors of the Geological Research Authority of the Sudan) for their strong support during our recent visits to the Sudan. As always, our appreciation goes to the people of the Sudan for their unfailing courtesy, hospitality and help. We dedicate this paper to the memory of Dr Françoise Gasse, friend and colleague, whose encouragement and shining example we will sorely miss: '*Atteindre au delà, chercher à s'élever toujours*'.

References

Abbate, E., Albianelli, A., Awad, A., Billi, P., Bruni, P., Delfino, M., Ferretti, M.P., Filippi, O., Gallai, G., Ghinassi, M., Lauritzen, S.-E., Lo Vetro, D., Martínez-Navarro, B., Martini, F., Napoleone, G., Bedri, O., Papini, M., Rook, L., Sagri, M., 2010. Pleistocene environments and human presence in the middle Atbara valley (Khashm Girba, Eastern Sudan). Palaeogeogr. Palaeoclimatol. Palaeoecol. 292, 12–34.

Abell, P.I., Hoelzmann, P., 2000. Holocene palaeoclimates in northwestern Sudan: stable isotope studies on molluscs. Glob. Planet. Change 26, 1–12.

Adamson, D.A., Clark, J.D., Williams, M.A.J., 1974. Barbed bone points from Central Sudan and the age of the "Early Khartoum" tradition. Nature 249, 120–123.

Adamson, D.A., Gasse, F., Street, F.A., Williams, M.A.J., 1980. Late quaternary history of the Nile. Nature 287, 50–55.

Adamson, D.A., Gillespie, R., Williams, M.A.J., 1982. Palaeogeography of the Gezira and of the lower Blue and White Nile valleys. In: Williams, M.A.J., Adamson, D.A. (Eds.), A Land between Two Niles. Quaternary Geology and Biology of the Central Sudan. A.A. Balkema, Rotterdam, pp. 165–219.

Adamson, D.A., Clark, J.D., Williams, M.A.J., 1987. Pottery tempered with sponge from the White Nile, Sudan. Afr. Archaeol. Rev. 5, 115–127.

Arkell, A.J., 1949. Early Khartoum. Oxford University Press, Oxford.

Arkell, A.J., 1953. Shaheinab. Oxford University Press, Oxford.

Ayliffe, D., Williams, M.A.J., Sheldon, F., 1966. Stable carbon and oxygen isotopic composition of early-Holocene gastropods from Wadi Mansurab, north-central Sudan. Holocene 6, 157–169.

Barrows, T.T., Almond, P., Rose, R., Fifield, L.K., Mills, S.C., Tims, S.G., 2013. Late pleistocene glacial stratigraphy of the Kumara-Moana region, West Coast of South Island, New Zealand. Quat. Sci. Rev. 74, 139–159.

Barrows, T.T., Williams, M.A.J., Mills, S.C., Duller, G.A.T., Fifield, L.K., Haberlah, D., Tims, S.G., Williams, F.M., 2014. A White Nile megalake during the last interglacial period. Geology 42, 163–166.

Blanchet, C.L., Tjallingii, R., Frank, M., Lorenzen, J., Reitz, A., Brown, K., Feseker, T., Brückmann, W., 2013. High- and low-latitude forcing of the Nile River regime during the Holocene inferred from laminated sediments of the Nile deep-sea fan. Earth Planet. Sci. Lett. 364, 98–110.

Cramp, A., O'Sullivan, G., 1999. Neogene sapropels in the Mediterranean: a review. Mar. Geol. 153, 11–28.

DeMenocal, P., Ortiz, J., Guilderson, T., Adkins, J., Sarnthein, M., Baker, L., Yarusinsky, M., 2000. Abrupt onset and termination of the African Humid Period: rapid climate responses to gradual insolation forcing. Quat. Sci. Rev. 19, 347–361.

Ducassou, E., Mulder, T., Migeon, S., Gonthier, E., Murat, A., Revel, M., Capotondi, L., Bernasconi, S.M., Mascle, J., Zaragosi, S., 2008. Nile floods recorded in deep Mediterranean sediments. Quat. Res. 70, 382–391.

Ducassou, E., Migeon, S., Mulder, T., Murat, A., Capotondi, L., Bernasconi, M., Mascle, J., 2009. Evolution of the Nile deep-sea turbidite system during the Late Quaternary: influence of climate change on fan sedimentation. Sedimentology 56, 2061–2090.
Duller, G.A.T., 2003. Distinguishing quartz and feldspar in single grain luminescence measurements. Radiat. Meas. 37, 161–165.
El Badri, O., 1972. Sediment Transport and Deposition in the Blue Nile at Khartoum, (Flood Seasons 1967, 1968 and 1969). Unpublished MSc thesis. University of Khartoum.
El Boushi, I.M., Abdel Salam, Y., 1982. Stratigraphy and ground-water geology of the Gezira Plain, central Sudan. In: Williams, M.A.J., Adamson, D.A. (Eds.), A Land between Two Niles. Quaternary Geology and Biology of the Central Sudan. A.A. Balkema, Rotterdam, pp. 65–80.
Fairbanks, R.G., Mortlock, R.A., Chiu, T.-C., Cao, L., Kaplan, A., Guilderson, T.P., Fairbanks, T.W., Bloom, A.L., Grootes, P.M., Nadeau, M.-J., 2005. Marine radiocarbon calibration curve spanning 0 to 50,000 years B.P. based on paired 230Th/234U/238U and 14C dates on pristine corals. Quat. Sci. Rev. 24, 1781–1796.
Foucault, A., Stanley, D.J., 1989. Late quaternary paleoclimatic oscillations in East Africa recorded by heavy minerals in the Nile delta. Nature 339, 44–46.
Galbraith, R.F., Roberts, R.G., Laslett, G.M., Yoshida, H., Olley, J.M., 1999. Optical dating of single and multiple grains of quartz from Jinmium Rock Shelter, Northern Australia: Part 1, experimental design and statistical models. Archaeometry 41, 339–364.
Galbraith, R.F., Green, P.F., 1990. Estimating the component ages in a finite mixture. Nucl. Tracks Radiat. Meas. 17, 197–206.
Garzanti, E., 2015. The Nile sediment system: processes and products (this volume). Quat. Sci. Rev. (in review).
Garzanti, E., Andò, S., Vezzoli, G., Abdel Megid, A.A., El Kammar, A., 2006. Petrology of Nile River sands (Ethiopia and Sudan): sediment budgets and erosion patterns. Earth Planet. Lett. 252, 327–341.
Gasse, F., 2000a. Water resources variability in tropical and subtropical Africa in the past. In: Water Resources Variability in Africa during the XXth Century. International Association of Hydrological Sciences Publication No. 252, pp. 97–105.
Gasse, F., 2000b. Hydrological changes in the African tropics since the Last Glacial Maximum. Quat. Sci. Rev. 19, 189–211.
Gasse, F., Chalié, F., Vincens, A., Williams, M.A.J., Williamson, D., 2008. Climatic patterns in equatorial and southern Africa from 30, 000 to 10, 000 years ago reconstructed from terrestrial and near-shore proxy data. Quat. Sci. Rev. 27, 2316–2340.
Hennekam, R., Jilbert, T., Schnetger, B., de Lange, G.J., 2014. Solar forcing of Nile discharge and sapropel S1 formation in the early- to mid-Holocene. Paleoceanography 29 (5). http://dx.doi.org/10.1002/2013PA002553.
Higgs, N.C., Thomson, J., Wilson, T.R.S., Croudace, I.W., 1994. Modification and complete removal of eastern Mediterranean sapropels by postdepositional oxidation. Geology 22, 423–426.
Hoelzmann, P., Gasse, F., Dupont, L.M., Salzmann, U., Staubwasser, M., Leuschner, D.C., Sirocko, F., 2004. Palaeoenvironmental changes in the arid and subarid belt (Sahara-Sahel-Arabian Peninsula) from 150 kyr to present. In: Battarbee, R.W., Gasse, F., Stickley, C.E. (Eds.), Past Climate Variability through Europe and Africa, vol. 6. Springer, Dordrecht, pp. 219–256.
Hurni, H., 1982. Hochgebirge von Semien – Äthiopien. In: Klima und Dynamik der Höhenstufung von der letzten Kaltzeit bis zur Gegenwart. Geographica Bernensia G 13, Beiheft 7 zum Jahrbuch der Geographischen Gesellschaft von Bern, p. 196.
Kieniewicz, J.M., Smith, J.R., 2007. Hydrologic and climatic implications of stable isotope and minor element analyses of authigenic calcite silts and gastropod shells from a mid-Pleistocene pluvial lake, Western Desert, Egypt. Quat. Res. 68, 431–444.
Krom, M.D., Stanley, D., Cliff, R.A., Woodward, J.C., 2002. River Nile sediment fluctuations over the past 7000 yr and their key role in sapropel development. Geology 30, 71–74.
Larrasoaña, J.C., Roberts, A.P., Rohling, E.J., Winklhofer, M., Wehausen, R., 2003. Three million years of monsoon variability over the northern Sahara. Clim. Dyn. 21, 689–698.
Lourens, L.J., Antonarakou, A., Hilgen, F.J., Van Hoof, A.A.M., Vergnaud-Grazzini, C., Zachariasse, W.J., 1996. Evaluation of the Plio-Pleistocene astronomical timescale. Paleoceanography 11, 391–413.
Macklin, M.G., Woodward, J.C., Welsby, D.A., Duller, G.A.T., Williams, F.M., Williams, M.A.J., 2013. Reach-scale river dynamics moderate the impact of rapid Holocene climate change on floodwater farming in the desert Nile. Geology 41, 695–698.
Marshall, M.H., Lamb, H.F., Huws, D., Davies, S.J., Bates, R., Bloemendal, J., Boyle, J., Leng, M.J., Umer, M., Bryant, C., 2011. Late Pleistocene and Holocene drought events at Lake Tana, the source of the Blue Nile. Glob. Planet. Change 78, 147–161.
Mawson, R., Williams, M.A.J., 1984. A wetter climate in eastern Sudan 2, 000 years ago? Nature 308, 49–51.
Mayewski, P.A., Rohling, E.E., Stager, J.C., Karlén, W., Maasch, K.A., Meeker, L.D., Meyerson, E.A., Gasse, F., van Kreveld, S., Lee-Thorp, J., Rosqvist, G., Rack, F., Staubwasser, M., Schneider, R.R., Steig, E.J., 2004. Holocene climate variability. Quat. Res. 62, 243–255.
McDougall, I., Brown, F.H., Fleagle, J.G., 2008. Sapropels and the age of hominins Omo I and II, Kibish, Ethiopia. J. Hum. Evol. 55, 409–420.
Mercone, D., Thomson, J., Abu-Zied, R.H., Croudace, I.W., Rohling, E.J., 2001. High-resolution geochemical and micropalaeontological profiling of the most recent eastern Mediterranean sapropel. Mar. Geol. 177, 25–44.
Murray, A.S., Olley, J.M., 2002. Precision and accuracy in the optically stimulated luminescence dating of sedimentary quartz: a status review. Geochronometria 21, 1–16.
Osmaston, H.A., Mitchell, W.A., Osmaston, J.A.N., 2005. Quaternary glaciation of the Bale Mountains, Ethiopia. J. Quat. Sci. 20, 593–606.
Padoan, M., Garzanti, E., Harlavan, Y., Villa, I.M., 2011. Tracing Nile sediment sources by Sr and Nd isotope signatures (Uganda, Ethiopia, Sudan). Geochem. Cosmochim. Acta 75, 3627–3644.
Praetorius, S.K., Mix, A.C., 2014. Synchronization of North Pacific and Greenland climates preceded abrupt deglacial warming. Science 345, 444–448.
Prescott, J.R., Hutton, J.T., 1994. Cosmic ray contributions to dose rates for luminescence and ESR dating: large depths and long-term time variations. Radiat. Meas. 23, 497–500.
Reinfelds, I., Swanson, E., Cohen, T., Larsen, J., Nolan, A., 2014. Hydrospatial assessment of streamflow yields and effects of climate change: snowy Mountains, Australia. J. Hydrol. 512, 206–220.
Revel, M., Ducassou, E., Grousset, F.E., Bernasconi, S.M., Migeon, S., Revillon, S., Mascle, J., Murat, A., Zaragosi, S., Bosch, D., 2010. 100,000 years of African monsoon variability recorded in sediments of the Nile margin. Quat. Sci. Rev. 29, 1342–1362.
Rodnight, H., Duller, G.A.T., Wintle, A.G., Tooth, S., 2006. Assessing the reproducibility and accuracy of optical dating of fluvial deposits. Quat. Geochronol. 1, 109–120.
Rohling, E.J., Pälike, H., 2005. Centennial-scale climate cooling with a sudden cold event around 8,200 years ago. Nature 434, 975–979.
Rohling, E., Abu-Zied, R., Casford, J., Hayes, A., Hoogakker, B., 2009. The marine environment: present and past. In: Woodward, J.C. (Ed.), The Physical Geography of the Mediterranean. Oxford University Press, Oxford, pp. 33–67.
Rossignol-Strick, M., 1985. Mediterranean quaternary sapropels, an immediate response of the African monsoon to variation of insolation. Palaeogeogr. Palaeoclimatol. Palaeoecol. 49, 237–263.
Rossignol-Strick, M., 1999. The Holocene climatic optimum and pollen records of sapropel 1 in the eastern Mediterranean, 9000-6000 BP. Quat. Sci. Rev. 18, 515–530.
Rossignol-Strick, M., Nesterhoff, W., Olive, P., Vergnaud-Grazzini, C., 1982. After the deluge: mediterranean stagnation and sapropel formation. Nature 295, 105–110.
Talbot, M.R., Williams, M.A.J., Adamson, D.A., 2000. Strontium isotope evidence for late Pleistocene reestablishment of an integrated Nile drainage network. Geology 28, 343–346.
Talbot, M.R., Williams, M.A.J., 2009. Cenozoic evolution of the Nile basin. In: Dumont, H.J. (Ed.), The Nile, Monographiae Biologicae, vol. 89. Springer, Dordrecht, pp. 37–60.
Thomson, J., Mercone, D., De Lange, G.J., Van Santvoort, P.J.M., 1999. Review of recent advances in the interpretation of eastern Mediterranean sapropel S1 from geochemical evidence. Mar. Geol. 153, 77–89.
Tothill, J.D., 1946. The origin of the Sudan Gezira clay plain. Sudan Notes Rec. 27, 153–183.
Tothill, J.D., 1948. A note on the origins of the soils of the Sudan from the point of view of the man in the field. In: Tothill, J.D. (Ed.), Agriculture in the Sudan. Oxford University Press, Oxford, pp. 129–143.
Verschuren, D., Sinninghe Damsté, J.S., Moernaut, J., Kristen, I., Blaauw, M., Fagot, M., Haug, G.H., CHALLACEA project members, 2009. Half-precessional dynamics of monsoon rainfall near the East African Equator. Nature 462, 637–641.
Welsby, D.A. (Ed.), 2001. Life on the Desert Edge: Seven Thousand Years of Human Settlement in the Northern Dongola Reach, Sudan. SARS, London.
Welsby, D.A., Macklin, M.G., Woodward, J.C., 2002. Human responses to Holocene environmental changes in the Northern Dongola reach of the Nile, Sudan. In: Friedman, R. (Ed.), Egypt and Nubia: Gifts of the Desert. British Museum Press, London, pp. 28–38.
Willcocks, W., 1904. The Nile in 1904. E. & F.N. Spon, London, p. 225.
Williams, M.A.J., 1966. Age of alluvial clays in the western Gezira, Republic of the Sudan. Nature 211, 270–271.
Williams, M.A.J., 1968a. Soil salinity in the west central Gezira, Republic of the Sudan. Soil Sci. 105 (6), 451–464.
Williams, M.A.J., 1968b. The influence of salinity, alkalinity and clay content on the hydraulic conductivity of soils in the west central Gezira. Afr. Soils 13 (1), 35–60.
Williams, M.A.J., 1968c. A dune catena on the clay plains of the west central Gezira, Republic of the Sudan. J. Soil Sci. 19 (2), 367–378.
Williams, M.A.J., 1969. Prediction of rainsplash erosion in the seasonally wet tropics. Nature 222, 763–765.
Williams, M.A.J., 1976. Erosion in the Alligator Rivers area. In: Lands of the Alligator Rivers Area, Northern Territory. CSIRO Land Research Series No. 38, pp. 112–125. Melbourne.
Williams, M.A.J., 1978. Water as an eroding agent. In: Howes, K.M.W. (Ed.), Studies of the Australian Arid Zone. III. Water in Rangelands, pp. 79–89.
Williams, M.A.J., 2009. Late Pleistocene and Holocene environments in the Nile basin. Glob. Planet. Change 69, 1–15.

Williams, M.A.J., 2014. Climate Change in Deserts: Past, Present and Future. Cambridge University Press, New York, p. 629.
Williams, M.A.J., Adamson, D.A., 1973. The physiography of the central Sudan. Geogr. J. 139, 498–508.
Williams, M.A.J., Adamson, D.A., 1974. Late Pleistocene desiccation along the White Nile. Nature 248, 584–586.
Williams, M.A.J., Adamson, D.A., 1980. Late quaternary depositional history of the Blue and White rivers in central Sudan. In: Williams, M.A.J., Faure, H. (Eds.), The Sahara and the Nile. A.A. Balkema, Rotterdam, pp. 281–304.
Williams, M.A.J., Adamson, D.A. (Eds.), 1982. A Land between Two Niles: Quaternary Geology and Biology of the Central Sudan. A.A.Balkema, Rotterdam, p. 246.
Williams, M., Nottage, J., 2006. Impact of extreme rainfall in the central Sudan during 1999 as a partial analogue for reconstructing early Holocene prehistoric environments. Quat. Int. 150, 82–94.
Williams, M.A.J., Talbot, M.R., 2009. Late quaternary environments in the Nile basin. In: Dumont, H.J. (Ed.), The Nile, Monographiae Biologicae 89. Springer, Dordrecht, pp. 61–72.
Williams, M., Jacobsen, G.E., 2011. A wetter climate in the desert of northern Sudan 9900-7600 years ago. Sahara 22, 7–14.
Williams, M.A.J., Medani, A.H., Talent, J.A., Mawson, R., 1974. A note on upper quaternary mollusca west of Jebel Aulia. Sudan Notes Rec. 54, 168–172.
Williams, M.A.J., Street, F.A., Dakin, F.M., 1978. Fossil periglacial deposits in the Semien Highlands, Ethiopia. Erdkunde 32, 40–46.
Williams, M.A.J., Adamson, D.A., Abdulla, H.H., 1982. Landforms and soils of the Gezira: a Quaternary legacy of the Blue and White Nile rivers. In: Williams, M.A.J., Adamson, D.A. (Eds.), A Land between Two Niles: Quaternary Geology and Biology of the Central Sudan. A.A. Balkema, Rotterdam, pp. 111–142.
Williams, M.A.J., Adamson, D.A., Cock, B., McEvedy, R., 2000. Late quaternary environments in the White Nile region, Sudan. Glob. Planet. Change 26, 305–316.
Williams, M.A.J., Adamson, D.A., Prescott, J.R., Williams, F.M., 2003. New light on the age of the White Nile. Geology 31, 1001–1004.
Williams, M., Talbot, M., Aharon, P., Abdl Salaam, Y., Williams, F., Brendeland, K.I., 2006. Abrupt return of the summer monsoon 15, 000 years ago: new supporting evidence from the lower White Nile valley and Lake Albert. Quat. Sci. Rev. 25, 2651–2665.
Williams, M.A.J., Usai, D., Salvatori, S., Williams, F.M., Zerboni, A., Maritan, L., Linseele, V., 2015. Late quaternary environments and prehistoric occupation in the lower White Nile valley, central Sudan. Quat. Sci. Rev. http://dx.doi.org/10.1016/j.quascirev.2015.03.007.
Williams, M.A.J., Williams, F.M., Duller, G.A.T., Munro, R.N., El Tom, O.A.M., Barrows, T.T., Macklin, M., Woodward, J., Talbot, M.R., Haberlah, D., Fluin, J., 2010. Late quaternary floods and droughts in the Nile Valley, Sudan: new evidence from optically stimulated luminescence and AMS radiocarbon dating. Quat. Sci. Rev. 29, 1116–1137.
Wintle, A.G., Murray, A.S., 2006. A review of quartz optically stimulated luminescence characteristics and their relevance in single-aliquot regeneration dating protocols. Radiat. Meas. 41, 369–391.
Wohl, E., 2011. A World of Rivers: Environmental Change on Ten of the World's Great Rivers. University of Chicago Press, Chicago, p. 359.
Woodward, J.C., Macklin, M.G., Welsby, D.A., 2001. The Holocene fluvial sedimentary record and alluvial geoarchaeology in the Nile Valley of Northern Sudan. In: Maddy, D.M., Macklin, M.G., Woodward, J.C. (Eds.), River Basin Sediment Systems: Archives of Environmental Change. A. A. Balkema, Abingdon, pp. 327–356.
Zhao, Y., Colin, C., Liu, Z., Paterne, M., Siani, G., Xie, X., 2012. Reconstructing precipitation changes in northeastern Africa during the quaternary by clay mineralogical and geochemical investigations of Nile deep-sea fan sediments. Quat. Sci. Rev. 57, 58–70.
Zhao, Y., Liu, Z., Colin, C., Paterne, M., Siani, G., Cheng, X., Duchamp-Alphonse, S., Xie, X., 2011. Variations of the Nile suspended discharges during the last 1.75 Myr. Palaeogeogr. Palaeoclimatol. Palaeoecol. 311, 230–241.